Lithos 246–247 (2016) 134–148

Contents lists available at ScienceDirect

Lithos

journal homepage: www.elsevier.com/locate/lithos

Geochronology and geochemistry of zircon from the northern Western Gneiss Region: Insights into the Caledonian tectonic history of western Norway

Stacia M. Gordon [a,*], Donna L. Whitney [b], Christian Teyssier [b], Haakon Fossen [c], Andrew Kylander-Clark [d]

[a] Department of Geological Sciences, University of Nevada, Reno, NV 89557, USA
[b] Department of Earth Sciences, University of Minnesota, Minneapolis, MN 55455, USA
[c] Department of Earth Science and Museum of Natural History, University of Bergen, N-5020 Bergen, Norway
[d] Department of Earth Science, University of California, Santa Barbara, CA 93106, USA

ARTICLE INFO

Article history:
Received 6 September 2015
Accepted 25 November 2015
Available online 17 December 2015

Keywords:
Western Gneiss Region
Zircon
Split-stream
LA-ICPMS
Distribution coefficients

ABSTRACT

The Western Gneiss Region (WGR) of Norway is divided by the Møre-Trøndelag shear zone (MTSZ) into a southern region that contains domains of Caledonian ultrahigh-pressure (UHP) metamorphic rocks (>2.5 GPa) and a northern area of similar Caledonian-aged rocks that record a maximum pressure reported thus far of ~1.5 GPa. Although both regions contain similar lithologies (primarily migmatitic quartzofeldspathic gneiss containing mafic lenses) and structural relationship of basement rocks to infolded nappes, this difference in maximum pressure implies a difference in tectonic history (continental subduction south of the shear zone, none to the north) and raises questions about the role of the MTSZ in the metamorphic history (including exhumation) of the WGR. Previous geochronology results indicated a difference in timing of peak metamorphism (older in north, younger in south). In order to better understand the tectonic history of the northern WGR and the MTSZ, and in particular the late- to post-Caledonian tectonic history, U–Pb zircon geochronology and trace-element abundances were obtained using the split-stream, laser-ablation ICPMS technique from metabasaltic lenses and migmatitic quartzofeldspathic host rocks from the structurally lowest exposed region of the northern WGR (Roan Peninsula basement), as well as leucosomes from an intercalated portion of the Seve Nappe Complex and a pegmatite in the MTSZ. Zircon from Roan gneiss and metabasite yield metamorphic ages of ca. 410–406 Ma, and zircon from a variety of migmatite samples (foliation-parallel leucosome to dikes) indicate melt crystallization at ca. 410 to 405 Ma. The Seve Nappe leucosomes yield only early Caledonian dates that cluster at ca. 437 Ma and ca. 465 Ma, suggesting that the allochthons in this region did not experience (or record) the same Scandian tectonic history as the basement rocks. Zircon from a weakly deformed pegmatite dike within the MTSZ crystallized at ca. 404 Ma, indicating that this shear zone was active during the end-stages of high-grade metamorphism in both the southern and northern WGR domains. Results of this study show that the northern and southern WGR experienced a coeval Scandian metamorphic, magmatic and deformation history, despite a possible difference in maximum P–T conditions.

1. Introduction

The Western Gneiss Region (WGR) of Norway (Fig. 1) is well known as a giant ultrahigh-pressure (UHP) terrane that experienced continental subduction to mantle depths during the Paleozoic Caledonian orogeny. Eclogite-facies conditions, including coesite eclogite and locally, diamond-bearing eclogite and gneiss, have been documented over large areas (>25,000 km^2) (e.g., DesOrmeau et al., 2015; Hacker et al., 2010; Hacker et al., 2015; Holder et al., 2015; Krogh et al., 2011; Kylander-Clark et al., 2007, 2008, 2009; Root et al., 2005; Terry et al., 2000a, b; Vrijmoed et al., 2006; Wain, 1997; Walsh et al., 2007). However, although both the northern and southern WGR show the same outcrop relationships of metabasite lenses enclosed within migmatitic gneiss (Fig. 2), only the southern part of the WGR contains a record of UHP metamorphism. This may indicate a significant tectonic discontinuity from north to south across the Møre-Trøndelag shear zone, a sinistral strike-slip shear zone that marks the boundary between the northern and southern WGR (Fig. 1B).

Another apparent difference between the southern and northern WGR is the age of metamorphism. Numerous geochronology studies of the southern WGR have shown that the main stage of Scandian (U)HP metamorphism occurred between ~425–400 Ma (DesOrmeau et al., 2015; Hacker et al., 2015; Krogh et al., 2011; Kylander-Clark et al., 2007, 2008; Terry et al., 2000b; Walsh et al., 2007). In contrast, in the northern WGR, where there has been much less geochronologic

* Corresponding author.
E-mail address: staciag@unr.edu (S.M. Gordon).

http://dx.doi.org/10.1016/j.lithos.2015.11.036
0024-4937/

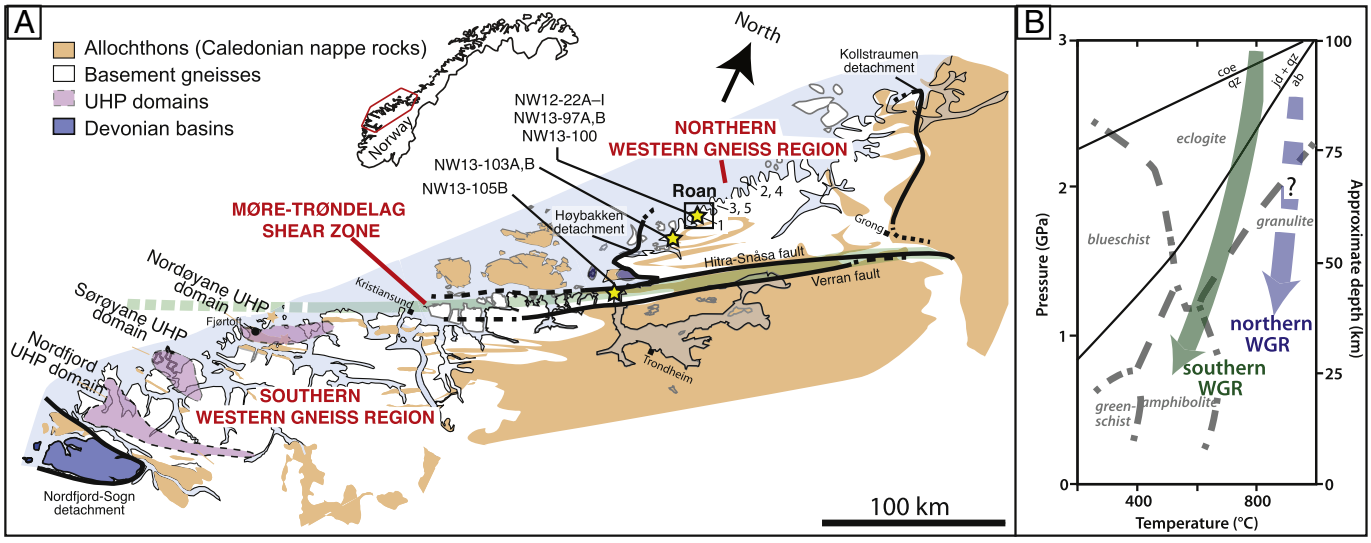

Fig. 1. (A) Simplified geologic map of the Western Gneiss Region, Norway showing the southern, ultrahigh-pressure domain and the northern domain, separated by the Møre-Trøndelag shear zone (after Braathen et al. (2000) and Fossen (2010)). Note the intercalated nature of the basement and the Allochthons along the western coast of Norway. The stars represent the location of analyzed samples, and the box shows the location of the map in Fig. 3. Also shown are the locations of the previously dated metabasite and dike samples (indicated by the numbers in the northern WGR), including: 1) Sm–Nd cpx–opx–grt–whole rock isochron age of 432 ± 6 Ma from a Roan metabasalt (Dallmeyer et al., 1992); 2) zircon U–Pb age of 434 ± 22 Ma for a leucosome (Schouenborg et al., 1991); 3) a late pegmatite at 404 ± 2 Ma (zircon U–Pb; Schouenborg et al., 1991); 4) a folded pegmatite at 401 ± 3 Ma (zircon U–Pb; Schouenborg, 1988); and 4) a late (nondeformed) pegmatite at 398 ± 3 Ma (zircon U–Pb; Dallmeyer et al., 1992). (B) Pressure–temperature diagram showing the general differences between the pressure/temperature history of the southern and northern WGR domains. The P–T path for the northern domain is based on data from Roan Peninsula metabasites and is bracketed by the 870 °C, 1.45 GPa P–T estimates of Johansson and Möller (1986). Texturally early clinopyroxene + garnet ± kyanite observed in some Roan metabasites suggests the rocks may have experienced an earlier higher pressure history.

work, one study of a metabasaltic pod in migmatite from the structurally deepest exposed level reported an Sm–Nd isochron age of 432 Ma (Dallmeyer et al., 1992).

As part of understanding why the northern and southern WGR seem to differ in at least part of their tectonic history, it is necessary to understand the timing of metamorphism, partial melting/crystallization, magmatism (represented by granitic dikes), and deformation in and beyond the Møre-Trøndelag shear zone. Although the southern WGR has been extensively studied, the P–T–t history of the northern WGR has not been as well documented. In this study, we present new split-stream, laser-ablation ICPMS zircon results from mafic and leucocratic rocks exposed within the northern WGR and from a deformed pegmatite in the MTSZ to track the metamorphic and melt-crystallization history and to determine a minimum age for MTSZ motion. Moreover, as the WGR basement rocks are commonly complexly intercalated with overlying allochthonous units, two Seve Nappe Complex leucosomes were also analyzed to compare their metamorphic and melt-crystallization history with that of the basement rocks, providing data for further comparison between the northern and southern WGR.

A significant result of this study is that the northern and southern WGR record coeval metamorphism, melt crystallization, and deformation. This finding can be used to guide future investigations of possible variations in the P–T history between different segments of giant (U)HP terranes such as the WGR, and the possible role of shear zones such as the Møre-Trøndelag.

2. Geologic setting

The Scandinavian Caledonides formed as a result of the Cambro–Silurian closure of the Iapetus Ocean and collision of Laurentia and Baltica in the late Silurian (Gee, 1975). This continent–continent collisional event, on the scale of Alpine–Himalayan orogenesis, caused 1) the amalgamation and translation of a series of thrust sheets to the E–SE (the Lower, Middle, Upper, and Uppermost Allochthons; Roberts

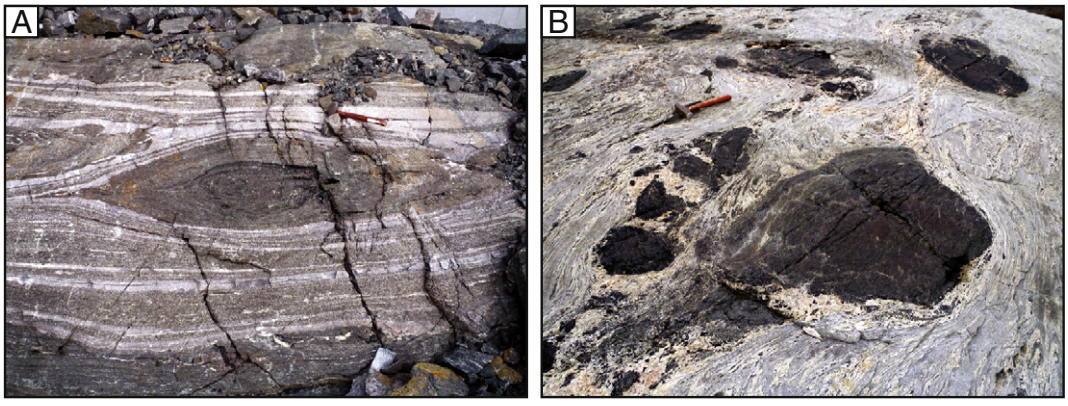

Fig. 2. Outcrop photographs from the (A) southern WGR and (B) northern WGR showing meter-scale metabasite lenses within migmatitic, quartzofeldspathic gneiss.

and Gee, 1985); and 2) during the end-stages of orogenesis, the subduction and UHP metamorphism of part of the Baltica basement and overlying nappes (e.g., Gee, 1975; Walsh et al., 2007). Throughout the Scandinavian Caledonides, numerous windows through the Allochthons expose the basement rocks (Roberts, 2003; Roberts and Gee, 1985). In many areas, thrust imbrication and later extensional deformation, including folding, has resulted in the juxtaposition and tight interfolding of the nappes and basement rocks particularly along the western coast of Norway (Gee, 1980; Krill, 1980; Tucker, 1986; Robinson, 1995; Braathen et al., 2000; Robinson and Hollocher, 2008a).

2.1. Western Gneiss Region

The Western Gneiss Region (WGR) is a window into the Baltica basement (Fig. 1) and represents the deepest exposed structural level of the Scandinavian Caledonides (e.g., Gee, 1975). The WGR consists mainly of polymetamorphosed, migmatitic quartzofeldspathic gneiss (the Western Gneiss Complex) that formed from ~1690 to 1620 Ma and was later reworked during Sveconorwegian (1100–950 Ma) and Caledonian orogenesis (500–405 Ma) (e.g., Fossen, 2010) (Fig. 2a). High-grade metamorphism (including eclogite-facies metamorphism) occurred during the final stages of Scandian collision and during the early stages of the following extension/exhumation (~425–400 Ma; Gee, 1975; Fossen, 2000).

The eclogites exposed throughout the southern WGR have received the most study because this region represents one of the largest and best-exposed ultrahigh-pressure (UHP) terranes on Earth. The UHP eclogites are found within three discrete areas, the Nordfjord, Sørøyane, and Nordøyane domains (Fig. 1; Wain, 1997; Root et al., 2005; Vrijmoed et al., 2006; Hacker et al., 2010). Overall, the eclogites show a SE to NW increase in P–T conditions, from 700 °C, ~2.8 GPa in the southern, Nordfjord UHP domain to 850 °C, 3.2–3.6 GPa in the northern, Nordøyane UHP domain (Cuthbert et al., 2000; Hacker, 2006; Krogh, 1977; Ravna and Terry, 2004; Young et al., 2007). Moreover, maximum P–T conditions may have been as high as 7 GPa and 1000 °C, based on the occurrence of majoritic garnet and the Al content of orthopyroxene in some metaperidotite bodies (Scambelluri et al., 2008; van Roermund, 2009). The increase in P–T conditions to the northwest is also reflected in an overall increase in the abundance of leucosomes and migmatization toward the northwest in the southern WGR (Hacker et al., 2010).

Across the three UHP domains of the southern WGR, eclogite-facies metamorphism has been proposed to have occurred from 425 to 400 Ma, followed by a lower-pressure (1.5–0.5 GPa), amphibolite-facies overprint at 400–385 Ma (DesOrmeau et al., 2015; Hacker et al., 2015; Holder et al., 2015; Krogh et al., 2011; Kylander-Clark et al., 2007, 2008; Terry et al., 2000b; Walsh et al., 2007). Melt crystallization in different generations of leucosomes and granitic dikes was coeval with the end stages of eclogite-facies metamorphism (~410–400 Ma) and continued during decompression and cooling of the UHP terrane (~400–375 Ma) (Ganzhorn et al., 2014; Gordon et al., 2013; Krogh et al., 2011; Kylander-Clark and Hacker, 2014; Schärer and Labrousse, 2003). By ~375 Ma, the rocks had cooled below ~400 °C ($^{40}Ar/^{39}Ar$ muscovite dates; Hacker and Gans, 2005; Root et al., 2005; Walsh et al., 2013). There is some disagreement about the exhumation mechanism/modes, but most agree that the southern WGR was exhumed as a coherent slab (e.g., Andersen et al., 1991; Brueckner and Cuthbert, 2013; Kylander-Clark et al., 2009).

The northern WGR, also termed the Vestranden Gneiss and the Central Norway Basement Window, exhibits the same outcrop relationships as seen in the southern WGR (e.g., metabasite enclosed within migmatitic quartzofeldspathic gneiss; Fig. 2b) and has been refolded on a regional scale into domal structures (Birkeland, 1958; Kjerulf, 1871; Ramberg, 1943, 1966). Some metabasites in the structurally lowest part of the northern WGR (Roan Peninsula; Fig. 3) experienced moderately high-pressure/high-temperature metamorphism in the stability

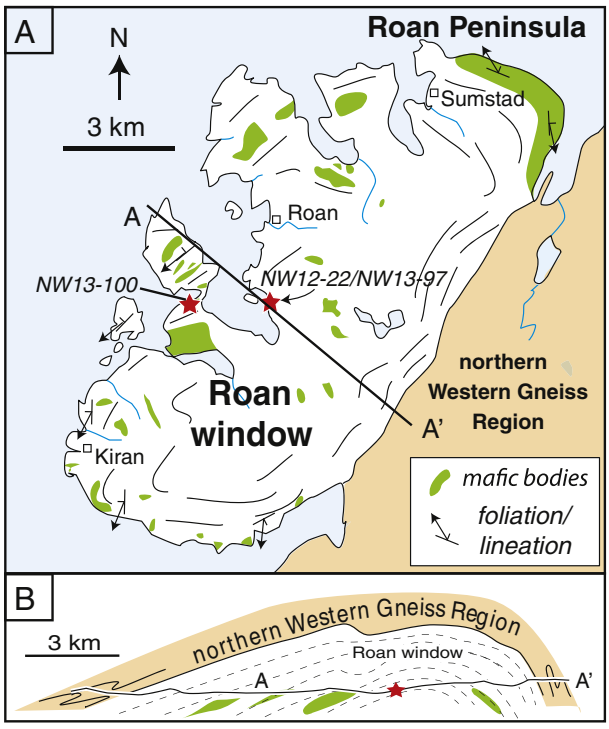

Fig. 3. (A) Simplified geologic map of the Roan Peninsula within the northern WGR (after Johansson and Möller (1986), Möller (1988), and Gilotti and Hull (1993)), showing the location of the metabasite within the dominantly quartzofeldspathic host gneiss. Red stars indicate the location of the dated samples; (B) cross-section through the Roan Peninsula (see A for location).

field of kyanite (Johansson and Möller, 1986; Möller, 1988). These contain an early garnet + clinopyroxene ± kyanite assemblage that has been partially replaced by orthopyroxene + plagioclase ± amphibole + sapphirine + corundum. Johansson and Möller (1986) used thermobarometry on a plagioclase-free garnet + clinopyroxene + orthopyroxene ± amphibole + rutile metabasite to obtain a P–T estimate of 870 ± 50 °C at 1.45 ± 0.2 GPa. This metamorphism is interpreted to have occurred at 432 ± 6 Ma based on a Sm–Nd cpx–opx–grt–whole rock isochron age from a Roan metabasalt (Dallmeyer et al., 1992), and a zircon U–Pb age determined for a leucosome from the northern Vestranden region (434 ± 22 Ma; Schouenborg et al., 1991; Fig. 1). Similar to the UHP rocks to the south, the Roan rocks underwent near-isothermal decompression and reequilibrated at amphibolite-facies conditions (Möller, 1988). Hornblende and muscovite $^{40}Ar/^{39}Ar$ ages from northern WGR rocks indicate exhumation through ~400 °C by 390 ± 2 Ma (Dallmeyer et al., 1992).

As in the southern WGR, the Roan Peninsula rocks are highly migmatitic and show multiple generations of melt, some of which were likely generated in situ, whereas later generations clearly were intrusive (Figs. 3, 4); partial melting and retrogression (amphibolitization) also affected metabasaltic lithologies (Figs. 2B, 4A). Limited previous geochronometric work has been done on these melt generations in the northern WGR: three dikes have been dated using U–Pb zircon geochronometry throughout the northern WGR (Fig. 1), revealing a wide range of ages: a late pegmatite at 404 ± 2 Ma (Schouenborg et al., 1991), a folded pegmatite at 401 ± 3 Ma (Schouenborg, 1988), and a late (nondeformed) pegmatite at 398 ± 3 Ma (Dallmeyer et al., 1992).

Overall, the Roan Peninsula rocks are very similar in field relations, composition and texture to those exposed within the southern WGR (Fig. 2). Notably, however, the northern WGR does not contain the abundant peridotite and other ultramafic rocks that are found throughout the southern WGR (e.g., Brueckner, 1969; Brueckner et al., 2002; van Roermund and Drury, 1998).

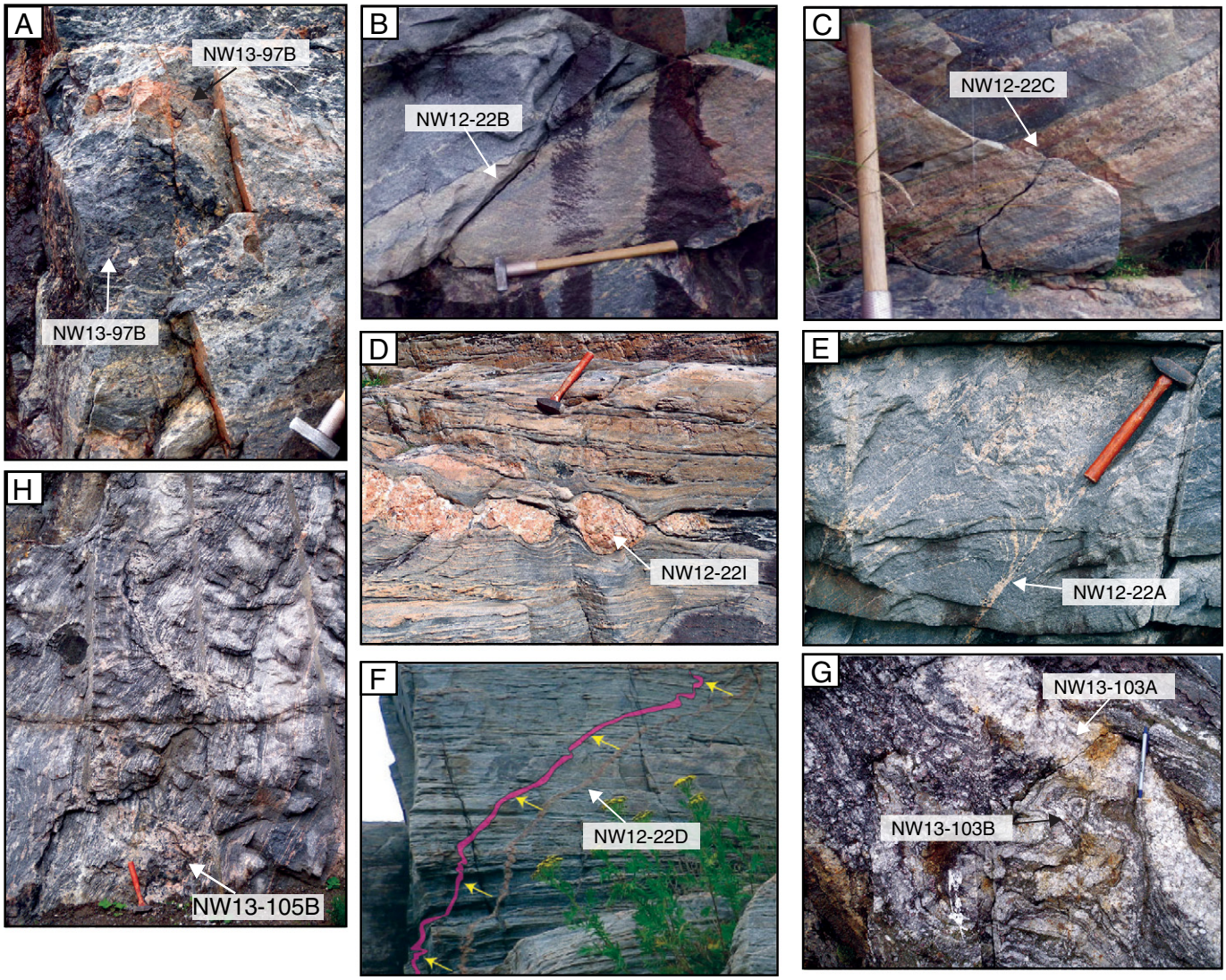

Fig. 4. Outcrop photographs of the samples studied here: (A) garnet amphibolite NW13-97A and gray gneiss NW13-97B; (B) fine-grained granitic leucosome NW12-22B; (C) foliation-parallel granitic leucosome NW12-22C; (D) boudinaged granitic pegmatite NW12-22I; (E) leucosome collected in a shear band NW12-22A; (F) weakly folded dike NW12-22D (pink line is an outline of the dike for clarity); (G) folded, foliation-parallel leucosome NW13-103B and folded, cross-cutting pegmatite NW13-103A; and (H) weakly deformed pegmatitic dike NW13-105B.

2.2. Seve Nappe Complex

Along the western coast of Norway, the WGR rocks both north and south of the MTSZ, are infolded with supracrustal units of the Allochthons, and in particular the Seve Nappe Complex, also called the Blåhø Nappe, of the Middle Allochthon. The Seve Nappe Complex represents the rifted Baltoscandian margin and contains continent–ocean transition zone rocks (Andréasson and Gee, 2008; Gee et al., 2013).

Within the northern Seve Nappe Complex, many investigations of the Seve Nappe Complex have focused on two regions in Sweden: Norrbotten and Jämtland. These areas contain early Caledonian HP to UHP eclogite and gneiss (Brueckner and van Roermund, 2004; Janák et al., 2013; Mørk et al., 1988; van Roermund, 1985; van Roermund and Bakker, 1984), including the recent discovery of diamond (Majka et al., 2014); (U)HP metamorphism has been dated at ~505–475 Ma (Norbotten; Mørk et al., 1988; Stephens and van Roermund, 1984; Essex et al., 1997; Root and Corfu, 2012) and ~460–446 Ma (Jämtland; Brueckner and van Roermund, 2007; Root and Corfu, 2012). A younger tectonomagmatic event at ~442–428 Ma is recognized in the Jämtland Seve Nappe rocks, and this event produced multiple generations of leucosome and pegmatite (Ladenberger et al., 2014; Majka et al., 2012).

Within the southern WGR, the diamond-bearing Fjørtoft gneiss (Dobrzhinetskaya et al., 1995) has been interpreted to represent the Blåhø Nappe (Terry et al., 2000a, b), which is considered to be part of the Seve Nappe Complex (e.g., Robinson, 1995). In the northwestern area of the southern WGR, mapping of the basement rocks reveals that they are narrowly infolded within the Seve Nappe (Fig. 1; Terry et al., 2000a), as is observed in the northern WGR. Monazite ages from the Fjørtoft gneiss suggest that the Seve Nappe Complex in the southern WGR underwent UHP metamorphism from ~415–407 Ma (Terry et al., 2000b). Walsh et al. (2007) dated multiple Seve Nappe Complex metapelites from mainly east of the Nordfjord and Sørøyane UHP domains, and zircon from one sample yielded a concordia age of 480 ± 12 Ma, whereas monazite revealed Caledonian ages from ~500 to 385 Ma. These results were used to argue that the allochthons were emplaced onto the Baltica basement prior to subduction and (U)HP metamorphism.

Overall, the rocks are strongly deformed (Gee et al., 2013). Thus, the Seve Nappe and WGR 'basement' rocks, where in contact

and interfolded, show very similar textural and metamorphic relationships.

2.3. Møre-Trøndelag Shear Zone

The southern and northern parts of the WGR, along with the associated infolded supracrustal rocks, are separated by the MTSZ (Fig. 1). The MTSZ is a steep, complex strike-slip shear zone that acted as a ductile shear zone that accommodated sinistral transtension in the Early Devonian (e.g., Braathen et al., 2000; Fossen et al., 2013; Krabbendam and Dewey, 1998; Osmundsen et al., 1998; Roberts, 1983). This structure was involved in at least the late-stage exhumation of the high-grade rocks exposed in the WGR to the north and south of the shear zone (Braathen et al., 2000; Krabbendam and Dewey, 1998). The rocks within the MTSZ are complex and have been interpreted in multiple ways: 1) the Gula Group of the Trondheim Nappe or Köli Nappe (Wolff, 1976); or 2) reworked Western Gneiss Complex basement (Tucker et al., 2004). The host rock intruded by the pegmatite analyzed in this study appears to be the typical migmatitic quartzofeldspathic basement gneiss observed throughout the WGR.

3. Methodology

To investigate the timing of metamorphism and melt crystallization in the northern WGR, we analyzed a total of 11 samples (Figs. 1, 3, 4; Table 1). Eight samples from the Roan Peninsula were analyzed: two metabasites, one gneiss, four leucosomes, and one granitic dike all collected within the mapped "Proterozoic gneiss" body exposed throughout the Roan Peninsula. In addition, we analyzed three samples from two other localities: one pegmatite that intruded basement gneiss within the MTSZ, and a leucosome and a pegmatite from a kyanite–garnet migmatite in the Seve Nappe exposed between the Roan Peninsula and the MTSZ (Fig. 1).

Zircon was extracted from the samples, using standard mineral-separation techniques, mounted, and imaged via cathodoluminescence (CL) (Fig. S1). For the leucosome samples, zircons were only extracted from the leucosome; the mesosome was carefully avoided. The CL images revealed internal zonation that was used to guide the LA-ICPMS analyses. For all the zircon analyses, the laser-ablation system at the UC-Santa Barbara ICPMS facility was operated in split-stream mode, in which half of the ablated material was sent to a *Nu Plasma* multicollector-ICPMS (MC-ICPMS) and the other half of the material to an *Agilent 7700x* quadrupole ICPMS (see summary of technique in Kylander-Clark et al., 2013). Furthermore, a *Photon Machines Analyte* 193 laser-ablation system was used for the analyses. The laser fluence was ~3–4 J/cm^2 for all analyses, producing an ablation rate of 0.05–0.10 μm/pulse, and a typical pit depth of ~7 μm. The spot size was 20–30 μm depending upon the size of the zircon.

The U–Th–Pb isotopic zircon results, collected on the MC-ICPMS, are presented in standard concordia diagrams for the Caledonian-age zircons (Figs. 5, 7; U–Pb Redux 2.50, Bowring et al., 2011; McLean et al., 2011). Results are also described in Table S1. All errors are reported at the two-sigma level and typically are ± 8–9 Myr for these Caledonian ages (Table S1). Uncertainties associated with all the geochronometric dates are a combination of analytical and propagated uncertainty, which accounts for the long-term standard reproducibility of ~2% for the standards run during all sessions on the instruments. Where the MSWD suggests a single population, weighted-average ages and associated errors are reported.

Trace-element abundances were collected simultaneously with the U–Th–Pb isotopic measurements on an *Agilent* quadrupole ICPMS as described above. The rare-earth element results are shown on standard REE diagrams, normalized to chondrite (Figs. 6, 8; Sun and McDonough, 1989), and in Table S3. In addition, because garnet can play a major role in controlling the trace-element abundances in a rock (i.e., the heavy REEs), in situ laser-ablation line transects were performed to measure the trace-element abundances and zoning within individual garnet crystals from the two Roan metabasites and the gneiss. The analyses were done also using the *Agilent* quadrupole ICPMS at UC-Santa Barbara. The results are shown in Fig. 9 and Table S2.

4. Results

4.1. Zircon split-stream analyses

To understand the timing of metamorphism, melt crystallization, and deformation within the Roan Peninsula, we targeted an outcrop that preserves metabasite pods hosted within migmatitic

Table 1
Studied metabasite, leucosomes, and pegmatites from the northern WGR.

Sample Number	UTM	location	Rock	Mineral	Scandian $^{206}Pb/^{238}U$ Dates
			Type	Assemblage	(Ma)[a]
NW13-97A	557216, 7113682	Roan Peninsula	Garnet amphibolite	Garnet, hornblende, biotite, plag, sphene, apatite, ilmenite	ca. 417 to 395 Ma; WMA: 406.4 ± 8.1 Ma (MSWD = 2.6; n = 32)
NW13-97B	557216, 7113682	Roan Peninsula	Gray gneiss	Quartz, plagioclase, biotite, apatite, titanite, ilmenite	ca. 415 to 405 Ma; WMA: 410.3 ± 8.2 Ma (MSWD = 1.6; n = 17)
NW12-22A	557216, 7113682	Roan Peninsula	Hornblende-bearing leucosome pooled within a vein-like shear band	Quartz, plagiocalse, hornblende	ca. 411 to 399 Ma; WMA: 404.1 ± 8.1 Ma (MSWD = 1.9; n = 28)
NW12-22B	557216, 7113682	Roan Peninsula	Fine-grained, granitic leucosome with cuspate margins	Quartz, plagioclase, k'spar, biotite, garnet	ca. 415 to 406 Ma; WMA: 408.6 ± 8.2 Ma (MSWD = 0.88; n = 5)
NW12-22C	557216, 7113682	Roan Peninsula	Strongly folded hornblende-bearing granitic leucosome	Quartz, plagioclase, k'spar, biotite, hornblende, garnet	ca. 417 to 401 Ma; WMA: 410.3 ± 8.2 Ma (MSWD = 2.3; n = 29)
NW12-22D	557216, 7113682	Roan Peninsula	Folded, hornblende-bearing dike	Quartz, plagiocalse, k'spar, minor biotite	ca. 417 to 401 Ma; WMA: 407.3 ± 8.1 Ma (MSWD = 1.3; n = 84)
NW12-22I	557216, 7113682	Roan Peninsula	Foliation-parallel, boundinaged granitic pegmatite	Quartz, plagioclase, k'spar, biotite	ca. 433 to 395 Ma; WMA: 405.3 ± 8.1 Ma (MSWD = 2.1; n = 47)
NW13-100	557573, 7114911	Roan Peninsula	Granulite	Garnet, opx, plagioclase, amphibole, biotite, ilmenite	ca. 416 Ma
NW13-103a	546472, 7087831	Førsholman	Folded, cross-cutting pegmatite	Garnet, biotite, plagioclase, quartz, kyanite, titanite	ca. 492 to 431 Ma; WMA: 435.9 ± 8.7 Ma (MSWD = 0.9; n = 6)
NW13-103b	546472, 7087831	Førsholman	Fine-grained, folded leucosome cut by NW13-103a	Garnet, biotite, plagioclase, quartz, kyanite, titanite	ca. 489 to 427 Ma; WMA: 438.8 ± 8.8 Ma (MSWD = 3.2; n = 13), 464.5 ± 9.3 Ma (MSWD = 1.5; n = 8)
NW13-105b	536647, 7054333	Selva; Møre-Trøndelag shear zone	Pegmatite	Quartz, plagioclase, k'spar, biotite, hornblende	ca. 488 to 388 Ma; WMA: 403.8 ± 8.1 Ma (MSWD = 2.1; n = 51)

[a] WMA = weighted-mean age.

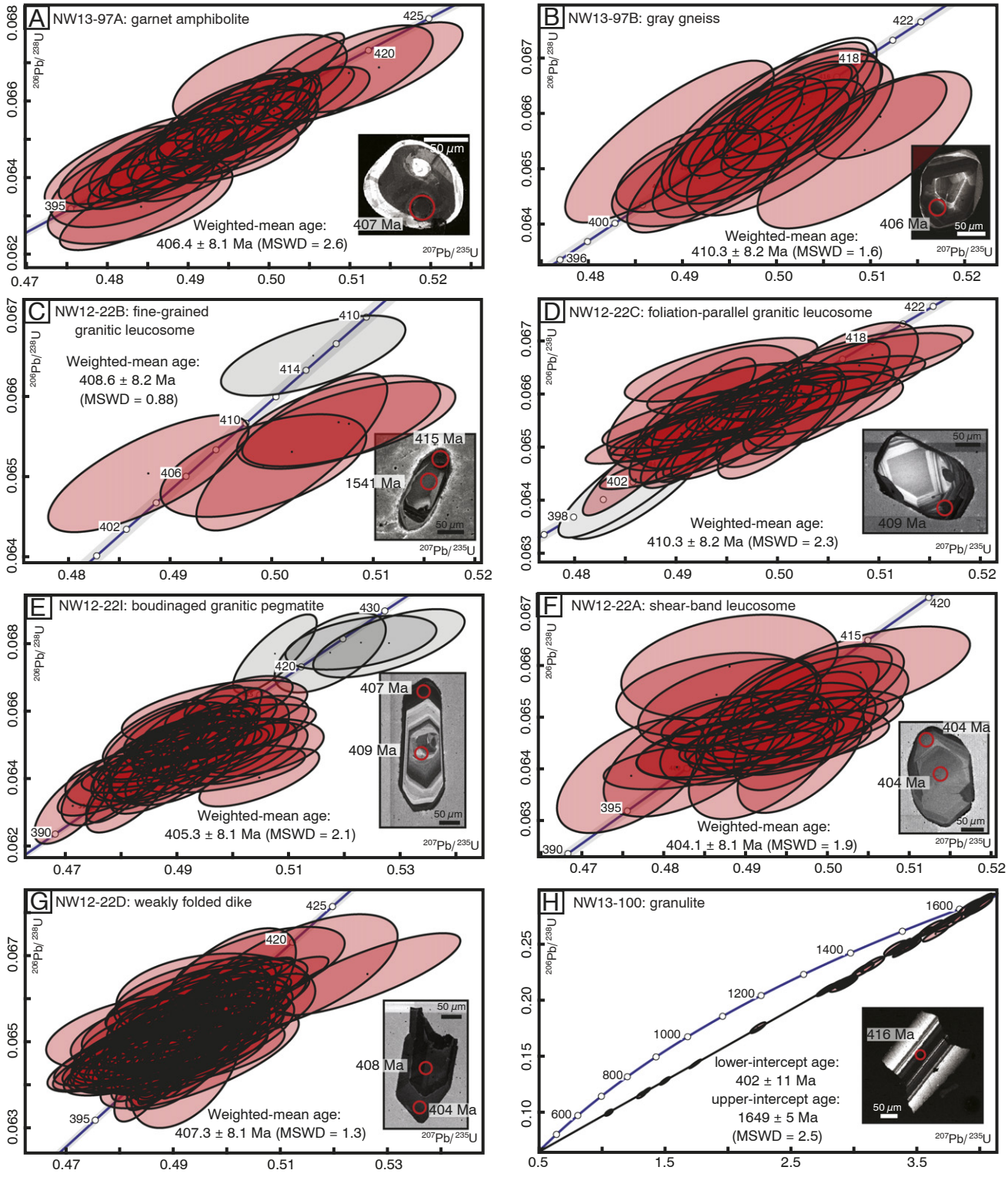

Fig. 5. Standard concordia diagrams showing the Scandian zircon ages from: (A) NW13-97A; (B) NW13-97B; (C) NW13-22B; (D) NW13-22C; (E) NW13-22I; (F) NW12-22A; (G) NW12-22D; and (H) NW13-100 (only one Scandian date was obtained from this sample so a concordia diagram is shown that includes the inherited zircon ages). Each ellipse represents a single spot analysis and its associated two-sigma error. Only the red ellipses are included in the calculated weighted-mean $^{206}Pb/^{238}U$ age. Inset in each diagram shows a representative CL image with the ablated regions shown by the red circle. The corresponding $^{206}Pb/^{238}U$ age is also shown. Dates are listed in Ma.

quartzofeldspathic gneiss that is cut by deformed granitic dikes (Fig. 4). The samples analyzed include: 1) a garnet-bearing amphibolite; 2) a gray gneiss that forms an ~30 cm thick corona around the amphibolite pod; 3) four leucosomes; and 4) one dike. The outcrop contains numerous meter-scale mafic pods and lenses; on some exposed surfaces of the outcrop, these appear to have formed from boudinaged mafic dikes. In addition, a grt-cpx metabasite containing texturally later orthopyroxene was collected from ~0.5 km west of the main targeted outcrop.

For all of these samples, both mafic and leucocratic, the U–Pb analyses reveal a ca. 1650 Ma upper-intercept age (Fig. S2). Most of the

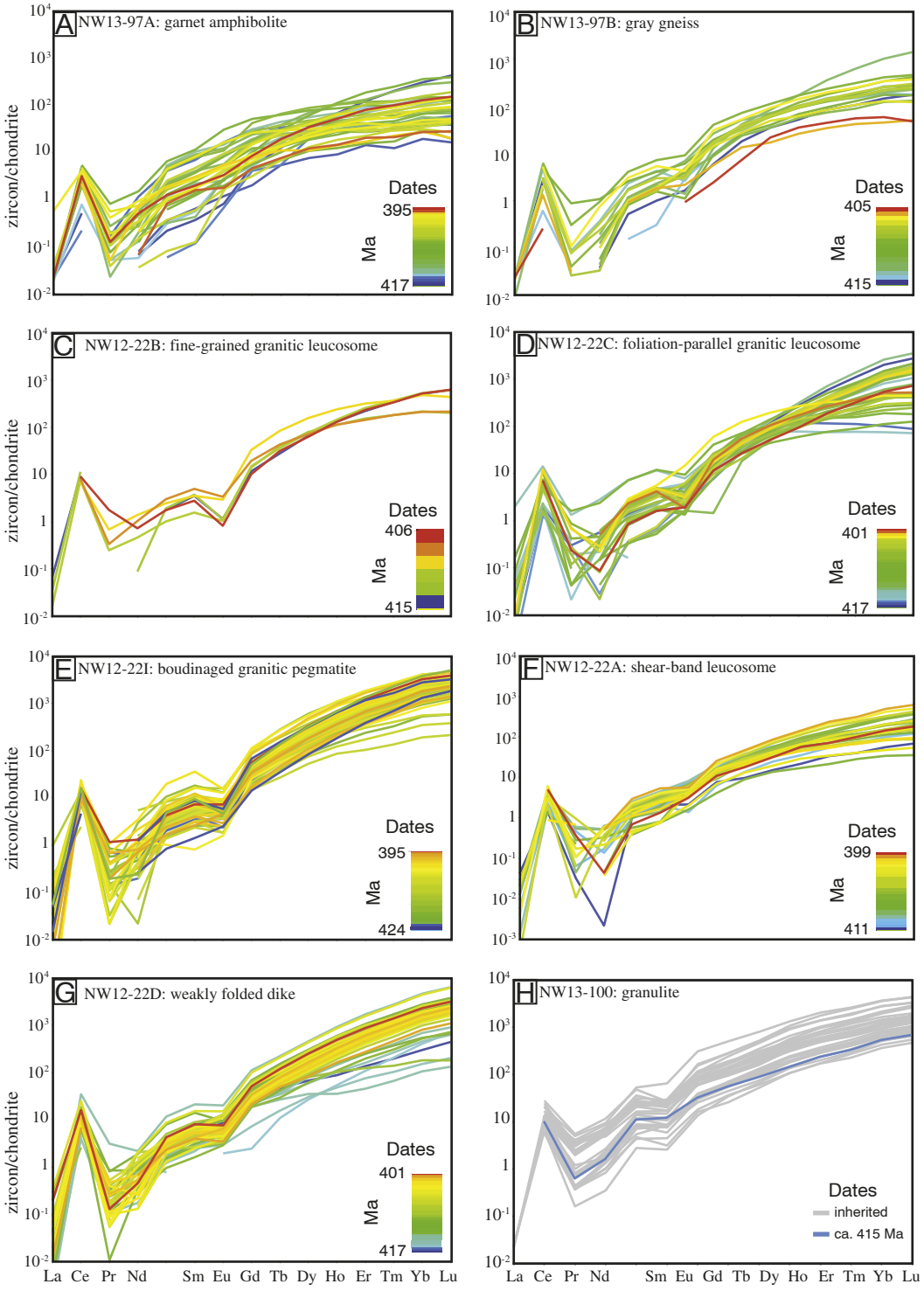

Fig. 6. Zircon rare earth element diagrams using the results from the Scandian zircons for samples: (A) NW13-97A; (B) NW13-97B; (C) NW13-22B; (D) NW13-22C; (E) NW13-22I; (F) NW12-22A; (G) NW12-22D; and (H) NW13-100 (as only one Scandian date was obtained from this sample, the REE pattern for the inherited zircons are also shown). Each line corresponds to a single ablated spot, and the lines are color-coded by the corresponding $^{206}Pb/^{238}U$ age. The zircons are normalized to chondrite (Sun and McDonough, 1989).

samples also yield Caledonian dates, and these are described for each sample below. Unless specified, the ages reported are weighted-mean $^{206}Pb/^{238}U$ ages.

The garnet amphibolite pod consists mainly of amphibole, garnet and plagioclase, with lesser amounts of biotite and quartz, and accessory titanite and zircon. Garnet has undergone significant retrogression and is typically surrounded by plagioclase rims. There is no evidence that melt infiltrated the mafic pod. The gray gneiss, in comparison, consists mainly of K-feldspar, plagioclase and quartz, with biotite and quartz ribbons defining a strong foliation. The garnet is skeletal in the gneiss and has significantly broken down.

From the garnet-amphibolite pod (sample NW13-97A; Fig. 4A), 32 analyzed zircons yield a weighted-mean average of 406.4 ± 8.1 Ma (MSWD = 2.6; Fig. 5A), and 17 zircons from the gray migmatitic gneiss

(NW13-97B) surrounding the mafic pod (Fig. 4A) reveal an age of 410.3 ± 8.2 Ma (MSWD = 1.6; Fig. 5B). The amphibolite zircons are rounded to elongate, with core and rim textures (Fig. S1). The rims typically show sector zoning and yielded the majority of the Scandian dates (Fig. 5A). They have relatively flat heavy rare-earth element (HREE) patterns (Lu_n/Dy_n = 1–6), and most zircons lack a negative Eu anomaly (Eu/Eu* = 0.5–1.7) (Fig. 6A). In comparison, the gray gneiss zircons are generally more prismatic, also show core and rim textures, but the rims show oscillatory zoning (Fig. 5B). The Scandian grains from the gray gneiss yield a similar REE pattern, with Lu_n/Dy_n of 2–6 and Eu/Eu* of 0.3–1.7 (Fig. 6B). The youngest grains (~405–406 Ma) yield a more flat HREE pattern in comparison to the cluster of zircons at ~410 Ma (Fig. 6B). The boundary between these two rocks is diffuse and intermingled (Fig. 4A).

The host quartzofeldspathic gneiss is strongly deformed, migmatitic, and crosscut by multiple generations of leucocratic dikes, all of which are deformed. Three leucocratic samples that are strongly deformed and parallel-to-subparallel to foliation were collected. Sample NW12-22B is a fine-grained granitic leucosome that has a biotite selvage, cuspate margins with the host gneiss, and has been transposed into the foliation (Fig. 4B). A second granitic leucosome (NW12-22C), which contains hornblende, was also transposed into the foliation and extensively folded and deformed (Fig. 4C). Zircons from NW12-22C are prismatic and typically contain low-U cores and high-U rims; both zones mainly show oscillatory zoning (Fig. S1). In comparison, zircons from NW12-22B are high-U, elongate, and have core and rim textures. The cores reveal either sector or oscillatory zoning, whereas the rims are oscillatory zoned. Zircons from these two early melt generations yield similar ages of 408.6 ± 8.2 Ma (MSWD = 0.88; n = 5) and 410.3 ± 8.2 (MSWD = 2.3; n = 29), respectively (Fig. 5C, D), with most of the Scandian dates revealed from the zircon rims. In comparison, NW12-22I is a boudinaged granitic pegmatite (Fig. 4D); zircons from this sample are also prismatic, with oscillatory-zoned cores and rims. The results are slightly younger, but within error of the strongly deformed leucosomes, with a weighted-mean age of 405.3 ± 8.1 Ma (MSWD = 2.1; n = 47; Fig. 5E).

In comparison with the amphibolite and gray gneiss, the majority of the leucosome zircons show steeper HREE patterns (Lu_n/Dy_n = 8–29), although zircons from all three leucosomes, in particular, NW12-22C, reveal some flat HREE patterns. The leucosomes also yield distinct negative Eu anomalies (Eu/Eu* = 0.2–0.6; with the exception of grains from NW12-22C that show some positive anomalies) (Fig. 6C, D, E). Leucosome NW12-22C shows the most variety in REE patterns, with some of the ca. 417–416 Ma zircons revealing flat HREE patterns and weak Eu anomalies (Fig. 6D). There is also another group of zircons that show intermediate HREE patterns and weak Eu anomalies, and a third group that shows steep HREE patterns and strong Eu anomalies. These three groups observed within NW12-22C zircons, however, do not correlate with age, grain size or grain texture.

Two leucocratic samples that crosscut the main foliation were also collected to track the later melting and deformation history. Sample NW12-22A is a hornblende-bearing leucosome that has in-filled a series of shear bands (Fig. 4E). Zircons from this leucosome are prismatic and show core and rim textures in CL images (Fig. S1). The cores contain sector and oscillatory zoning, whereas the rim overgrowths are typically oscillatory zoned. Like the more strongly deformed leucosomes, 28 zircons from NW12-22A reveal a similar age of 404.1 ± 8.1 (MSWD = 1.9) (Fig. 5F); the Scandian dates are mainly from zircon rims. The majority of these zircons show moderate HREE patterns (Lu_n/Dy_n = 2–7) and weak negative Eu anomalies (Eu/Eu* = 0.4–1.5) (Fig. 6F). Dike NW12-22D crosscuts the foliation, is continuous over several meters, and is gently folded (Fig. 4F). The zircons are homogeneous high-U grains with oscillatory zoning, and they yield a weighted-mean age of 407.3 ± 8.1 Ma (MSWD = 1.3; n = 84) (Fig. 5G). Moreover, the majority of the grains reveal a steep HREE slope (Lu_n/Dy_n = 6–26) and a negative Eu anomaly (Eu/Eu* = 0.3–0.8) (Fig. 6G). The older Scandian zircons (ca. 416–417 Ma) typically reveal a less steep HREE pattern.

In comparison with the analyzed garnet amphibolite pod, sample NW13-100 contains grt + cpx + (later) opx and minor late hornblende. Most of the garnet is euhedral to subhedral, contains abundant inclusions of kyanite, and has undergone minor retrogression, with thin plagioclase rims. Orthopyoxene is associated with plagioclase and interpreted to represent a later overprinting of the cpx + grt + ky assemblage. The mafic outcrop is a ~3 m long block in a region with abundant smaller mafic pods in garnet-bearing migmatitic hornblende gneiss; there is no evidence for melt infiltration or partial melting of the grt + cpx + opx mafic pod that was crushed for zircons. Of 31 zircons analyzed, only one shows a Scandian date of 416 ± 11 Ma (Fig. 5H), with a moderately steep HREE pattern (Lu_n/Dy_n = 8) and weak negative Eu anomaly (Eu/Eu* = 0.6) (Fig. 6H). All of the zircons were large (>200 μm) fragments, with sector zoning; the Scandian-age grain did not show any distinguishing properties compared to the older grains (Fig. S1).

South of the Roan Peninsula, closer to the Møre–Trøndelag shear zone (Fig. 1), the overall map pattern reveals prominently NE-plunging anticline and syncline hinges that expose the Baltica basement and supracrustal rocks of the Seve Nappe (Tucker et al., 2004). Near Førsholman, ~25 km SW of the Roan Peninsula, migmatitic metapelitic gneiss contains kyanite in both the mesosome and leucosome (Fig. 4G). The leucosome layers are quartz and plagioclase-rich, with lesser amounts of biotite, garnet and kyanite, whereas the mesosome contains more abundant, large, skeletal garnets with biotite and kyanite defining foliation and wrapping around the porphyroblasts. The kyanite and garnet in the leucosome are texturally similar to the mesosome and are not interpreted as peritectic phases. Two different generations of leucosome were collected, and the mesosome was avoided when the samples were crushed. Sample NW13-103B is a fine-grained, foliation-parallel leucosome that is folded. Sample NW13-103A is a pegmatite that cuts NW13-103B and is itself folded and strongly deformed. Both the leucosome and pegmatite have a similar composition, with kyanite and garnet present. Zircons from the samples are complicated, showing a wide range of textures. Typically in NW13-103B, the cores show sector zoning and the rims have oscillatory zoning; both zones are high U, gray in CL (Fig. S1). In comparison, CL images of the zircons from pegmatite NW13-103A reveal two different textural types: 1) low-U zircons with sector zoning; and 2) high-U grains with weak oscillatory zoning.

Both samples reveal a similar zircon age population that is distinct from the Roan Peninsula samples. The early leucosome, NW13-103B, contains a range of Caledonian zircons, from ~489 to 427 Ma, with 13 zircons yielding a weighted-mean age of 438.8 ± 8.8 Ma (MSWD = 3.2) and 8 zircons revealing an older weighted-mean age of 467.1 ± 9.3 Ma (MSWD = 2.5) (Fig. 7A). Most of the ~439 Ma zircons show a distinctly lower Lu_n/Dy_n ratio (average of 3) in comparison to the ~467 Ma population (average Lu_n/Dy_n = 15) (Fig. 8A). The Eu anomaly is similar between the age populations: Eu/Eu* ranging from 0.03 to 2.25 for the ~439 Ma population and 0.14 to 1.42 for the ~467 Ma population. The sector-zoned zircon cores typically yield the younger ~467 Ma younger age population, whereas the oscillatory rims yield the younger ~439 Ma age population (e.g., Fig. 7a; S1). The leucosome also yields Proterozoic zircons, with a group of ~780–670 Ma dates and individual concordant dates at ~1077 and 1586 Ma (Fig. S2).

In comparison, the pegmatite, NW13-103A, does not show any evidence for Proterozoic inheritance, with only early Caledonian-aged zircons that range from ~492 to 431 Ma (Fig. 7B). Similar to NW13-103B, 6 zircons from the pegmatite yield a weighted-mean age of 435.9 ± 8.7 Ma (MSWD = 0.91), which show the same flat HREE pattern (Lu_n/Dy_n = 0.9–1.2) and negative Eu anomaly (Eu/Eu* = 0.14–0.21) of the ~439 Ma zircon population from NW13-103B (Figs. 7B, 8B). The high-U, oscillatory-zoned zircons reveal this ~439 Ma population. The remaining low-U zircons yield steeper HREE patterns (Lu_n/Dy_n = 5–23) and older dates ~490 to 450 Ma. Notably,

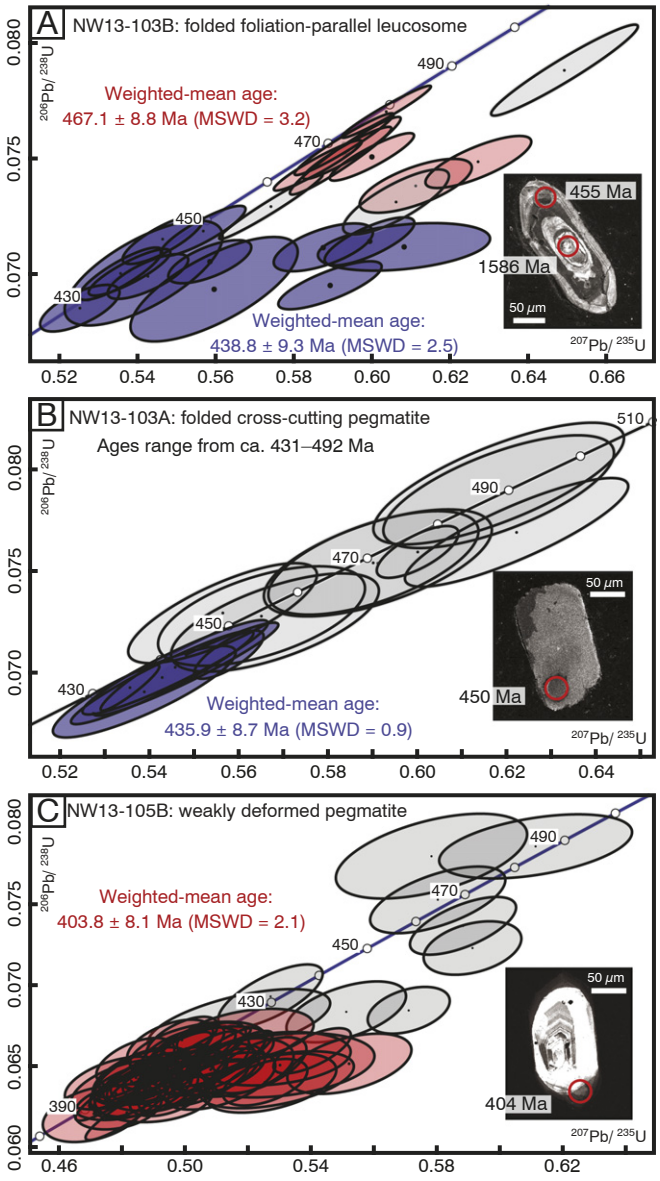

Fig. 7. Standard concordia diagrams showing the Caledonian zircon ages from: (A) NW13-103B; (B) NW13-103A; and (C) NW13-105B. Each ellipse represents a single spot analysis and its associated two-sigma error. Only the red or blue ellipses are included in the calculated weighted-mean $^{206}Pb/^{238}U$ age(s). Inset in each diagram shows a representative CL image with the ablated regions shown by the red circle. The corresponding $^{206}Pb/^{238}U$ age is also shown. Dates are listed in Ma.

no Scandian-aged zircons were found in either NW13-103A or -103B (Fig. 8B).

A granitic pegmatite sample, NW13-105B, was also collected within the Møre-Trøndelag shear zone near the town of Selva, ~60 km SW of the Roan Peninsula (Figs. 1, 4H). The pegmatite is partially deformed and transposed into the MTSZ foliation. The zircons are typically low-U (bright in CL), with thin, high-U rims (Fig. S1). Most of the zircons from NW13-105B yield a weighted-mean age of 403.8 ± 8.1 Ma (MSWD = 2.1; n = 51) (Fig. 7C). Where the rims were large enough, spots were placed on both the low- and high-U portions of the grains. Typically the high-U rims yield younger ages than the cores; however, the ages are typically within uncertainty of each other. Four additional zircons cluster at ~427 Ma, whereas five additional zircons yield concordant dates ranging from ~488 to 450 Ma (Fig. 7C). These grains do not show any textural or CL features that are unique from the Scandian-aged zircons. All of the zircons from this pegmatite reveal a steep HREE pattern (Lu_n/Dy_n = 59–277) and negative Eu anomaly (Eu/Eu* = 0.3–1.5) (Fig. 8C).

4.2. Garnet trace-element analyses

Garnets from the Roan amphibolite pod sample NW13-97A are typically small (50–200 μm), inclusion-free, with plagioclase coronas surrounding the grains. Given a spot size of 30 μm, only a single spot analysis was possible for some grains. The results show some differences among garnet grains (Fig. 9A; Table S2). Four garnets have flat HREE patterns (Lu_n/Dy_n = 0.7–0.9) and no negative Eu anomalies (Eu/Eu* = 1.01–1.19), whereas three other grains show steeper HREEs (Lu_n/Dy_n = 1.2–2.7) and weak negative Eu anomalies (Eu/Eu* = 0.53–0.78).

Garnets from the gray gneiss (NW13-97B) that surrounds the amphibolite vary in size, with two larger (0.5–0.8 mm) grains (grt 1 and 2) and two smaller (0.1–0.15 mm) grains (grt 3 and 4) analyzed for this study. The two larger grains are anhedral, whereas the smaller grains are more euhedral, but all are surrounded by plagioclase, suggesting they have broken down to some extent. Nearly all of the garnets yield distinct negative Eu anomalies (Eu/Eu* = 0.09–0.65) and mainly flat HREE patterns (Lu_n/Dy_n = 0.9–3.5) (Fig. 9B; Table S2). Individual grains have weak zoning, with slightly steeper HREE patterns in the garnet cores and mantles compared to the rims (Lu_n/Dy_n ratios for grt1m = 1.1 vs. grt1r = 0.9; grt2c = 2.7 vs. grt2r = 1.4; grt3c = 1.1 vs. grt3r = 0.9).

The grt–cpx rock, NW13-100, has the largest (~1–1.2 mm) and least retrogressed garnets; these grains contain abundant kyanite inclusions. The garnets from this rock show a distinct REE pattern compared to the amphibolite (Fig. 9C; Table S2). Garnet 1 shows strong core to rim zoning, with relatively flat HREE patterns in the garnet core (Lu_n/Dy_n = ~0.6) and rims that reveal negative HREE slopes (Lu_n/Dy_n = ~0.3). Garnet 2 has rims that have a more negative slope (Lu_n/Dy_n = 0.7) compared to the garnet core (Lu_n/Dy_n = 0.3). The third analyzed garnet does not show any zoning, but has a steep negative HREE slope (Lu_n/Dy_n = 0.1–0.9). There is no evidence for a negative Eu anomaly in any of the garnets (Eu/Eu* = 0.93–1.87).

4.3. Garnet/zircon partitioning

In order to evaluate if Scandian zircon grew under garnet-present conditions, the REE partitioning between garnet and zircon ($D_{REE(grt-zirc)}$) was calculated for the two metabasites and the migmatitic gray gneiss (Fig. 10). For the garnet from NW13-97A, we calculated an average garnet composition that yielded a flat HREE profile, and an average was calculated for the portion of the garnet that yielded the measured steep HREE pattern. Moreover, average garnet core and rim trace-element compositions were calculated for NW13-97B. These different garnet core and rim averages were paired with averages of the trace-element composition of zircon from these samples. As only one zircon in the grt–cpx rock (NW13-100) yielded a Scandian date, this zircon composition was paired with an average core and an average rim value from the garnets in this sample.

For the amphibolite (NW13-97A) $D_{REE(grt-zirc)}$ calculations, the pairing of the average zircon with the garnet that revealed the steep HREE pattern yielded values near unity for the MREE and dropped to a plateau at 0.10 for the HREE, thus favoring garnet for the HREE (Fig. 10A). In comparison, pairing the zircon with an average for the garnet that reveals a flat HREE pattern shows a moderate increase in slope from the middle to the heavy REEs.

For the migmatitic gray gneiss (NW13-97B), the $D_{REE(grt-zirc)}$ calculations are very similar for both garnet compositions, revealing a positive Eu anomaly, and a broad 'concave-up' shape for the remaining middle-to-heavy REEs (Fig. 10B). The pairing of the zircon with the garnet rim

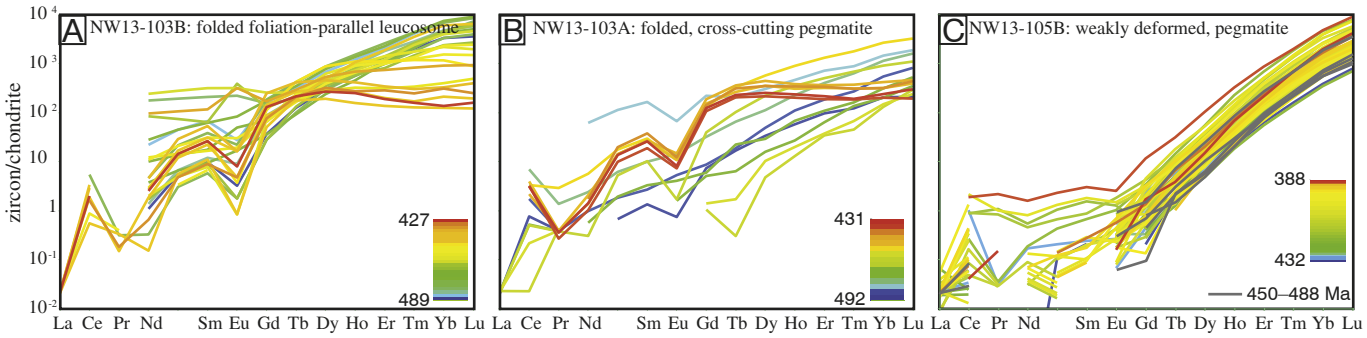

Fig. 8. Zircon rare earth element diagrams using the results from the Scandian zircons for samples: (A) NW13-103B; (B) NW13-103A; and (C) NW13-105B. Each line corresponds to a single ablated spot, and the lines are color-coded by the corresponding $^{206}Pb/^{238}U$ age. The zircons are normalized to chondrite (Sun and McDonough, 1989).

shows a similar pattern but a slight preferential partitioning of the HREE into zircon rather than garnet.

The $D_{REE(grt-zirc)}$ calculations for grt–cpx rock NW13-100 yield values above unity for the middle and heavy REE for zircon paired with both garnet core and rim values, and both pairings reveal a negative Eu anomaly (Fig. 10C). Furthermore, both sets show a steep slope for the middle-to-heavy REE suggesting significant partitioning ($D_{Lu(grt-zirc)} = 320$) of these elements into zircon. Moreover, the zircon paired with the garnet core shows a stronger partitioning of the HREE into zircon rather than garnet.

5. Discussion

The U–Pb zircon geochronology results for all of the Roan Peninsula samples, as well as the leucosomes from the Seve Nappe Complex and the pegmatite from within the MTSZ, reveal strong evidence for metamorphism and melt crystallization during the Caledonian. There are, however, some distinct differences in the timing of these events between the WGR basement versus the nappe samples. In the following sections, we compare the results obtained from the Seve Nappe Complex of the Middle Allochthon and Roan Peninsula samples to other regional northern WGR samples previously dated within these same units. Subsequently, we discuss how these results from the northern WGR compare to the extensively studied southern WGR.

5.1. Seve Nappe Complex

The leucosome (NW13-103B) and pegmatite (NW13-103A) collected from a migmatitic garnet–kyanite metapelite that is part of an intercalated portion of the Seve Nappe Complex with the basement rocks reveal nearly identical zircon results despite the fact that the folded pegmatite (NW13-103A) crosscuts the early, foliation-parallel leucosome (NW13-103B) (Figs. 4G, 7A, B). The early leucosome (NW13-103B) has some evidence of Proterozoic zircon inheritance, with zircon core ages ranging from ~1585 to 580 Ma, and this inherited signature is not found in the pegmatite (Fig. S2). Zircons from both samples record no evidence of Scandian metamorphism, but rather a wide range of early Caledonian dates from ~490–430 Ma. Within this range, two distinct zircon populations are present: ~437 Ma and ~467 Ma. In addition to these two Seve Nappe samples, the pegmatitic dike (NW13-105B) collected from within the MTSZ reveals similar early Caledonian ages, ~488–450 Ma (Fig. 7C). This inheritance pattern suggests that the protolith of the dike was from Seve Nappe Complex rocks.

The Seve Nappe leucosome and pegmatite studied here contain zircons that record nearly all of the metamorphic, migmatitic, and melt-crystallization events documented in the Norbotten and Jämtland Seve Nappe Complex rocks found to the east (Brueckner and van Roermund, 2007; Essex et al., 1997; Mørk et al., 1988; Root and Corfu, 2012; Stephens and van Roermund, 1984). The dominant zircon signature in both the leucosome and cross-cutting pegmatite at ~437 Ma likely records melt crystallization given the oscillatory zoning from the zircons that yielded these ages, and the similarity of these dates to a previously interpreted melt-crystallization event (Ladenberger et al., 2014; Majka et al., 2012). The trace-element signature revealed by the ~437 Ma zircons suggest that the zircons grew under garnet and plagioclase-stable conditions, with a flat HREE profile and distinct negative Eu anomaly (Fig. 8A, B).

The older dates observed in zircon cores and in some rims reveal different age patterns from the two samples, where the early leucosome records a distinct event at ca. 467 Ma and the pegmatite reveals a continuous spread of ages from ca. 490 to 450 Ma, with no clear population of dates (Fig. 7B). The ca. 467 Ma age population is slightly younger than the HP ages from the Norbotten region and slightly older than the (U)HP ages from the Jämtland region (Fig. 7A). Moreover, the trace-element signature of these zircons and from the pegmatite, suggests they grew under conditions in which garnet was not stable (i.e., a

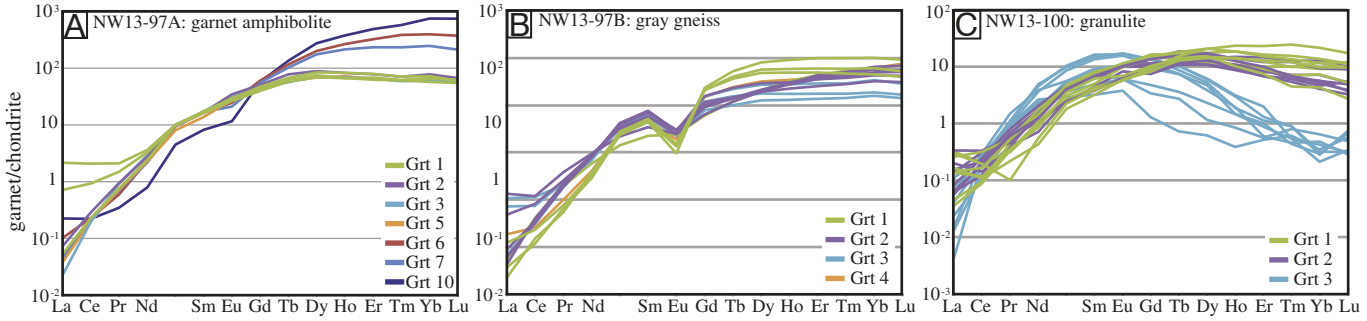

Fig. 9. Garnet rare earth element diagrams from metabasite and gray gneiss samples: (A) NW13-97A; (B) NW13-97B; and (C) NW13-100. The patterns are color-coded by individual garnets found in each sample. The garnets are normalized to chondrite (Sun and McDonough, 1989).

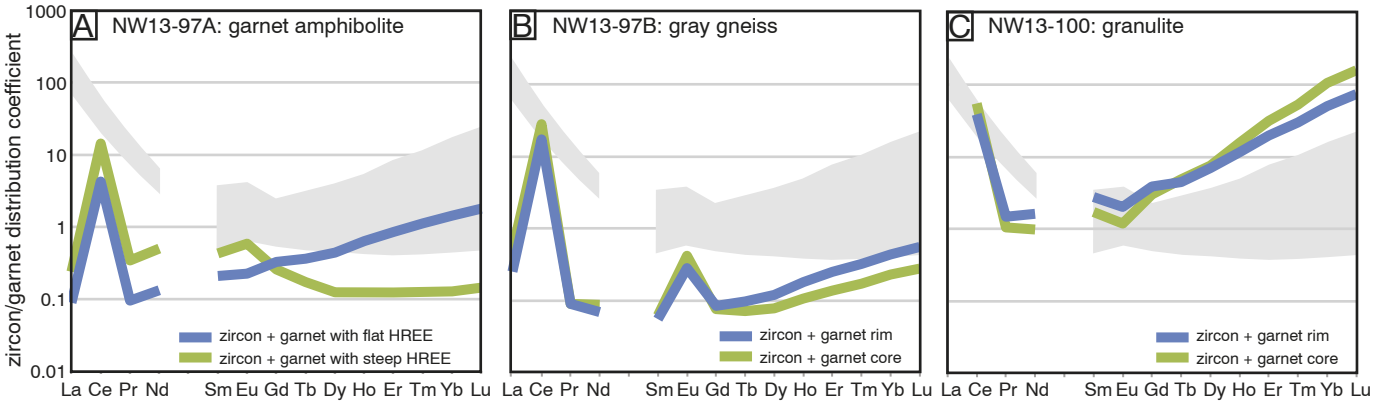

Fig. 10. Calculated distribution coefficients between zircon and garnet for the rare earth elements. Average zircon trace-element compositions are paired with different generations of garnet (based on its REE pattern). Also shown in the gray bar is the range of previously calculated experimental and empirical zircon/garnet partition coefficients (e.g., Baldwin et al., 2004; Harley et al., 2001; Hokada and Harley, 2004; Kelly and Harley, 2005; Monteleone et al., 2007; Rubatto, 2002; Rubatto and Hermann, 2003, 2007; Taylor et al., 2014; Whitehouse and Platt, 2003).

steep HREE slope) (Fig. 8A, B). Thus, the ca. 467 Ma leucosome age and the spread in ages from 490 to 450 Ma in the pegmatite may record the continuation of metamorphism between the two HP events. Alternatively, these Early Caledonian zircons may be inherited.

Our results, although based on only a few samples, may indicate a fundamental difference in the history of the Seve Nappe Complex exposed north and south of the MTSZ. To the south, the Seve Nappe rocks experienced Scandian metamorphism (Terry et al., 2000a, b; Walsh et al., 2007), whereas in the north, either new zircon growth in the Seve Nappe rocks did not take place during Scandian orogenesis, or the folding of the Seve Nappe rocks and the basement did not occur until late- or post-Scandian times. In addition, the leucosome and pegmatite also may be recording a new or continued metamorphic and/or melt crystallization event that had not been previously documented in the northern WGR Seve Nappe rocks at ca. 467 Ma. Alternatively, the samples may not be part of the Seve Nappe; however, more detailed mapping and isotopic analyses of the Allochthonous rocks exposed throughout the northern WGR are necessary to evaluate the basement versus nappe samples exposed throughout the region.

5.2. Northern WGR basement

Roan metabasite, migmatitic gneiss, and dikes reveal a strong record of mid- to late(post)-Scandian metamorphism, deformation, and melt crystallization similar to the timing of these events in the southern WGR (Figs. 5, 11; e.g. Andersen et al., 1991; Tucker et al., 1990, 2004; Terry et al., 2000a; Schärer and Labrousse, 2003; Root et al., 2004, 2005; Hacker, 2007; Kylander-Clark et al., 2007, 2008, 2009; Krogh et al., 2011; Gordon et al., 2013; Spencer et al., 2013; Kylander-Clark and Hacker, 2014). Both the Roan grt–cpx rock (NW13-100) and the garnet amphibolite (NW13-97A) samples contain zircons with weak to no negative Eu anomalies, and a weakly positive slope for the HREE patterns (Fig. 6A, H). The $D_{REE(Zircon/Garnet)}$ patterns suggest that zircon grew when garnet with the flat HREE pattern was present in garnet amphibolite (Figs. 9A, 10A), whereas the single Caledonian zircon from the grt–cpx rock suggests that garnet was unstable during its growth at ~416 Ma. More data need to be collected from this sample to better understand its metamorphic history; however, the garnet amphibolite (NW13-97A) suggests that garnet-stable metamorphism occurred at ~405 Ma (Fig. 5A). This age is significantly younger than the previous metamorphic age of ~432 Ma from a grt–cpx rock from the Roan Peninsula (Dallmeyer et al., 1992) and thus suggests high-grade metamorphism lasted until the late Scandian.

The zircons from all the melt generations studied here contain oscillatory zoning in either the entire crystal or in the dated zircon rims. In addition, abundant zircon should grow during melt crystallization; therefore, the significant zircon-age populations found between 410 to 404 Ma likely indicate the timing of melt crystallization (Fig. 5B–G). The early melt generations, including the foliation-parallel granitic leucosomes and pegmatite (NW12-22B, C, I) reveal melt crystallization at ~410 to 405 ± 8 Ma (Fig. 5B–E). The later crystallization of melt within a shear band and a weakly folded dike overlap within uncertainty and reveal crystallization ages of ~404 and 407 ± 8 Ma, respectively (Fig. 5F, G). Thus, despite the fact that the dike crosscuts the strongly deformed, foliation-parallel granitic layers, these rocks all crystallized rapidly by ~404 Ma. The results from the multiple generations of crystallized melt (e.g., from the gray gneiss that surrounds the garnet amphibolite to foliation-parallel leucosomes to a weakly folded dike) suggest that abundant in situ melting and melt emplacement occurred and crystallized rapidly during the Scandian orogeny (Fig. 5B–G).

The majority of the zircon from these samples reveal similar steep HREE profiles, suggesting crystallization post-garnet breakdown. However, there are a mix of REE patterns observed more commonly in the earlier melt generations, including the gray gneiss and foliation-parallel leucosomes. The spread in HREE patterns in these samples does not correlate with age, except for the gray gneiss, where HREE patterns from the youngest ages (~405 Ma) suggest garnet-stable crystallization.

The similarity in ages from these samples implies that the northern WGR remained at high temperature (above the solidus) until late in the deformation history, before cooling and crystallization of all analyzed samples at essentially the same time. These results are consistent with the near-isothermal decompression path determined from mineral reactions and thermobarometry (e.g., Johansson and Möller, 1986; Möller, 1988).

Given the granitic composition of the leucosomes, pegmatites, and dikes (NW12-22A,B,C,D,I; Table 1), these rocks were likely sourced from the abundant host basement gneiss. There is also significant field evidence that in some cases, the pods of metabasite have also undergone partial melting at their margins, producing a more mafic composition rock, herein described as the gray gneiss (NW13-97B) (Figs. 2B, 4A). This melting or disaggregation of some metabasite likely occurred relatively early, as the gray gneiss generally forms a corona around the metabasite pod but moving away from the metabasite, becomes strongly deformed and shares the deformation observed within the host gneiss. Zircons from the Roan gray gneiss reveal crystallization at 410 ± 8 Ma (Fig. 5B). As described above, these zircons show a different CL pattern from the garnet amphibolite, with the amphibolite zircons revealing sector zoning whereas the gray gneiss zircons contain oscillatory zoning (Fig. 5B). The zircon REE signatures from the gray gneiss are similar to the garnet amphibolite (Fig. 6A, B); however, the $D_{REE(Zircon/Garnet)}$ suggests that the zircon was not in equilibrium with garnet when it

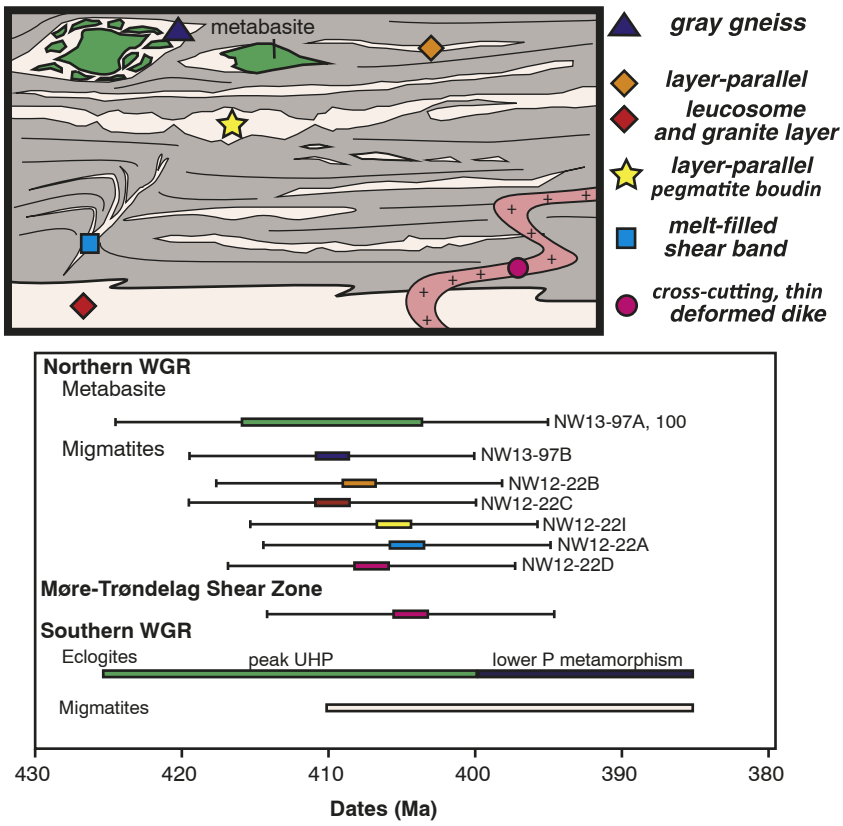

Fig. 11. Timeline of the metamorphic and melt-crystallization history of the southern and northern WGR and the Møre–Trøndelag shear zone. Also shown is a cartoon depicting the textural location of the different samples studied here. The weighted-mean age results and corresponding two-sigma errors are shown below in addition to the previously studied southern WGR (see Geologic Setting section for references for these ages) for reference. Note the similarity in ages from the northern versus the southern WGR.

crystallized (Fig. 10B), as the $D_{REE(Zircon/Garnet)}$ do not match with any of the experimental and natural data that suggests zircon–garnet equilibrium. Multiple sources for leucosomes have also been reported from the southern WGR. Ganzhorn et al. (2014) used leucosome compositions, experimental data, and multiphase-garnet inclusions to argue that both felsic gneiss and (ultra)mafic rocks underwent continuous(?) melting from high-pressure conditions through amphibolite-facies retrogression.

5.3. Comparison of the southern to the northern WGR

Previous petrologic and geochronometric studies from the northern WGR proposed an earlier high-pressure metamorphic history in comparison to the more extensively studied southern WGR (~432 Ma versus ~425–400 Ma, respectively) (Carswell et al., 2003; Glodny et al., 2008; Griffin and Brueckner, 1980, 1985; Johansson and Möller, 1986; Krogh et al., 2011; Kylander-Clark et al., 2007, 2009; Möller, 1988; Root et al., 2004; Terry et al., 2000b; Young et al., 2007). The results from this study, however, show that high-temperature metamorphism continued into the late Scandian and that this later metamorphism and melt crystallization were coeval across the entire WGR, with abundant migmatization and leucosome intrusion from ca. 410 to 400 Ma (Fig. 11; this study, Gordon et al., 2013; Kylander-Clark and Hacker, 2014).

Kyanite-bearing garnet–clinopyroxene rocks with later orthopyroxene (+ spinel + plagioclase) and, locally, corundum and sapphirine, occur in both the southern WGR (Butler et al., 2013; Hollocher et al., 2007; Straume and Austrheim, 1999) and northern WGR (Roan Peninsula: Johansson and Möller, 1986). In one such locality of the southern WGR (Ulsteinvik locality/central UHP domain), the P–T path involved isothermal decompression from > 2 GPa (eclogite facies) at 700–800 °C, with formation of the opx-bearing assemblage at 0.8–1.2 GPa (Straume and Austrheim, 1999). In the northern UHP domain of the southern WGR, the P–T path involved heating during decompression from 3 GPa at 760 °C to 1 GPa, ~810 °C (Butler et al., 2013). In the Roan area of the northern WGR, the conditions of garnet + clinopyroxene + orthopyroxene ± amphibolite + rutile assemblage have been estimated at ~1.45 GPa, 870 °C (Johansson and Möller, 1986). It is conceivable that higher pressures were attained, although more petrologic work is necessary to test this possibility.

The exhumation of the entire WGR occurred within an extensional tectonic regime, as evidenced by the tectonic windows of the southern and northern WGR being bounded by detachment-fault systems, including the Nordfjord–Sogn detachment in the south (e.g., Norton, 1986, 1987; Séranne and Séguret, 1987; Johnston et al., 2007) and the Høybakken–Kollstraumen detachment (e.g., Braathen et al., 2000, 2002; Séranne, 1992) to the north (Fig. 1). The Høybakken and Kollstrammen detachments exhumed the northern WGR in a manner similar to a metamorphic core complex (Braathen et al., 2000, 2002), whereas the southern WGR was likely exhumed from mantle depths as a relatively coherent slab by eduction and, secondarily and more efficiently, by the formation of a hinterland-dipping detachment zone (e.g., Fossen, 2000; Kylander-Clark et al., 2009). This differential exhumation was accommodated by sinistral shearing along the Møre–Trøndelag shear zone, which acted as a transfer fault between the two regions (Braathen et al., 2000; Séranne, 1992). The Devonian extension within an oblique divergent setting resulted in the simultaneous activity of these normal and sinistral strike-slip shear zones, deposition of large Devonian basins, and transtensional exhumation of the WGR (Andersen, 1998; Braathen et al., 2000; Dewey and Strachan, 2003; Fossen, 2010; Fossen et al., 2013; Krabbendam and Dewey, 1998; Osmundsen et al., 2006; Séranne, 1992; Torsvik et al., 1996).

Strain patterns consistent with transtensional exhumation (e.g., constrictional strain, lineation-parallel upright folds) developed

under amphibolite-facies conditions during the final stages of WGR exhumation (Dewey and Strachan, 2003; Fossen et al., 2013; Krabbendam and Dewey, 1998), but the switch from transpression to transtension may have occurred even earlier, potentially at (U)HP conditions (Renedo et al., 2015). Previous work (Fossen and Dunlap, 1998) suggests that the switch occurred around 405 Ma, assuming that it is recorded by the kinematic switch form thrusting to back-sliding (eduction) of the overlying orogenic wedge represented by the Jotun Nappe. Samples with contractional fabrics from the basal Caledonian thrust (décollement) zone yielded ca. 415–408 Ma Ar–Ar white mica and biotite dates, whereas samples exhibiting extensional fabrics yielded younger dates of ca. 402–395 Ma, bracketing the timing of the switch. The pegmatite studied here (NW13-105B) is weakly deformed but crosscuts the main host gneiss, which contains the dominant sinistral fabric produced due to MTSZ shearing. Zircons from this pegmatite yield a crystallization age of ca. 404 Ma (Fig. 7C), confirming that the MTSZ transfer zone was active while the northern WGR was undergoing metamorphism and melt crystallization and while the southern WGR was still at eclogite-facies (Carswell et al., 2003; Glodny et al., 2008; Griffin and Brueckner, 1980, 1985; Johansson and Möller, 1986; Krogh et al., 2011; Kylander-Clark et al., 2007, 2009; Möller, 1988; Root et al., 2004; Terry et al., 2000a, b; Young et al., 2007), further supporting that transtensional strain along this transfer fault was present early in the exhumation history of the WGR (Fig. 11). The ~404 Ma crystallization age is also coeval with the switch from thrusting to back sliding of the overlying orogenic wedge (Fossen and Dunlap, 1998).

Both the southern and northern WGR contain abundant evidence for migmatization and intrusion of melt (Figs. 2, 4), and the geochronometric results from both domains suggest that high strain developed under melt-present conditions (this study, Labrousse et al., 2002; 2011; Gordon et al., 2013; Ganzhorn et al., 2014). The presence of melt has significant rheological implications (e.g., Rosenberg and Handy, 2005; Rutter and Neumann, 1995) and could have induced bulk weakening across the WGR and/or allowed the subducted crustal material to detach from the subducting slab (e.g., Ganzhorn et al., 2014; Gordon et al., 2013; Labrousse et al., 2011), although recent models suggest that melting was an important influence likely only during the exhumation path of the WGR (Butler et al., 2015). While P–T differences between the southern and northern WGR cannot yet be comprehensively evaluated, during the mid-to-late Scandian, the southern and northern WGR domains shared the same history of metamorphism, deformation, and melt crystallization. The rheologic weakening induced by the presence of abundant melt within the northwestern portion of the southern WGR domain and in the northern WGR combined with simultaneous activity on a combination of normal (Nordfjord-Sogn, Høybakken, and Kollstraumen detachments) and strike-slip (MTSZ) faults aided in the exhumation of this giant high-grade terrane, exposing numerous windows into the deepest structural levels of the Scandinavian Caledonides (Fig. 12).

6. Conclusions

The new U–Pb zircon dates from metabasites, leucosomes, and dikes from the Roan Peninsula indicate that metamorphism and melt crystallization was coeval with the end stages (ca. 410–400 Ma) of eclogite-facies metamorphism and accompanying migmatization in the southern, UHP-portion of the WGR. However, the Seve Nappe leucocratic samples found intercalated with the basement rocks in the northern WGR show pre-Scandian ages, with no evidence of zircon recrystallization during the eclogite facies metamorphism in the southern WGR. These Seve Nappe samples thus show a much different history than the equivalent rocks found in the southern WGR domain that were emplaced on the basement rocks prior to subduction and (U)HP metamorphism. Overall, the southern and northern WGR basement rocks underwent significant migmatization within a transtensional tectonic setting. The buoyancy of this large high-grade metamorphic terrane as well as activity on a combination of normal and strike-slip faults, including the Møre–Trøndelag shear zone, added to the exhumation of the WGR within two domains beginning by at least ~404 Ma.

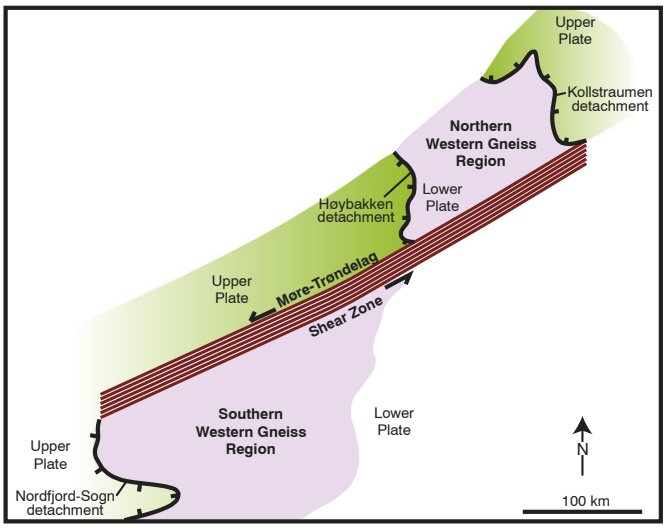

Fig. 12. Schematic diagram revealing the overall structural context of the northern and southern WGR (after Braathen et al., 2000). An oblique divergent tectonic system consists of a single detachment (the Nordfjord–Sogn detachment) that exhumes the (U)HP southern domain of the WGR and two detachments (the Kollstraumen–Høybakken system) that exhume the northern WGR, separated by the Møre–Trøndelag shear zone system. The results from this study reveal that the northern and southern WGR shared a similar Scandian metamorphic, magmatic, and deformation history.

Supplementary data to this article can be found online at http://dx.doi.org/10.1016/j.lithos.2015.11.036.

Acknowledgments

Hannes Brueckner and an anonymous reviewer provided very helpful comments and suggestions that greatly improved the manuscript. We would like to thank Joel DesOrmeau for his help with mineral separation and the LA-ICPMS analyses. We also thank Bradley Hacker for many insightful discussions and for his assistance in the UC-Santa Barbara ICPMS laboratory facility and Gareth Seward for his help in the UC-Santa Barbara SEM laboratory facility. This research was funded by NSF grants EAR-1062187 to Gordon and EAR-1040980 to Whitney and Teyssier.

References

Andersen, T.B., 1998. Extensional tectonics in the Caledonides of southern Norway, an overview. Tectonophysics 285, 333–351.
Andersen, T.B., Jamtveit, B., Dewey, J.F., Swensson, E., 1991. Subduction and eduction of continental crust: major mechanisms during continent–continent collision and orogenic extensional collapse, a model based on the south Norwegian Caledonides. Terra Nova 3, 303–310. http://dx.doi.org/10.1111/j.1365-3121.1991.tb00148.x.
Andréasson, P.G., Gee, D.G., 2008. The Baltica–Iapetus boundary in the Scandinavian Caledonides and a revision of the Middle and Upper Allochthons. International Geological Congress, 33rd, Oslo (Abstracts, v.1, p. EUR06601L).
Baldwin, S.L., Monteleone, B., Webb, L.E., Fitzgerald, P.G., Grove, M., Hill, E.J., 2004. Pliocene eclogite exhumation at plate tectonic rates in eastern Papua New Guinea. Nature 431, 263–267. http://dx.doi.org/10.1038/nature02846.
Birkeland, T., 1958. Geological and petrological investigations in northern Trøndelag, western Norway. Norsk Geologisk Tidsskrift 38, 327–420.
Bowring, J.F., McLean, N.M., Bowring, S.A., 2011. Engineering cyber infrastructure for U–Pb geochronology: Tripoli and U–Pb redux. Geochemistry, Geophysics, Geosystems 12, Q0AA19. http://dx.doi.org/10.1029/2010GC003479.
Braathen, A., Nordgulen, Ø., Osmundsen, P.-T., Andersen, T.B., Solli, A., Roberts, D., 2000. Devonian, orogen-parallel, opposed extension in the Central Norwegian Caledonides. Geology 28, 615–618.
Braathen, A., Osmundsen, P.T., Nordgulen, Ø., Roberts, D., Meyer, G., 2002. Orogen-parallel extension of the Caledonides in northern Central Norway: an overview. Norwegian Journal of Geology 82, 225–241.
Brueckner, H.K., 1969. Timing of ultramafic intrusions in the core zone of the Caledonides of southern Norway. Journal of American Sciences 267, 195–212.

Brueckner, H.K., Cuthbert, S.J., 2013. Extension, disruption, and translation of an orogenic wedge by exhumation of large ultrahigh-pressure terranes: examples from the Norwegian Caledonides. Lithosphere 5, 277–289. http://dx.doi.org/10.1130/L256.1.
Brueckner, H.K., van Roermund, H.L.M., 2004. Dunk tectonics: a multiple subduction/eduction model for the evolution of the Scandinavian Caledonides. Tectonics 23, TC2004. http://dx.doi.org/10.1029/2003TC001502.
Brueckner, H.K., van Roermund, H.L.M., 2007. Concurrent HP metamorphism on both margins of Iapetus: Ordovician ages for eclogites and garnet pyroxenites from the Seve Nappe Complex, Swedish Caledonides. Journal of the Geological Society, London 164, 117–128.
Brueckner, H.K., Carswell, D.A., Griffin, W.L., 2002. Paleozoic diamonds within a Precambrian peridotite lens in UHP gneisses of the Norwegian Caledonides. Earth and Planetary Science Letters 203, 805–816.
Butler, J.P., Jamieson, R.A., Steenkamp, H.M., Robinson, P., 2013. Discovery of coesite–eclogite from the Nordøyane UHP domain, Western Gneiss Region, Norway: field relations, metamorphic history, and tectonic significance. Journal of Metamorphic Geology 31, 147–163. http://dx.doi.org/10.1111/jmg.12004.
Butler, J.P., Beaumont, C., Jamieson, R.A., 2015. Paradigm lost: buoyancy thwarted by the strength of the Western Gneiss Region (ultra)high-pressure terrane, Norway. Lithosphere http://dx.doi.org/10.1130/L426.1.
Carswell, D.A., Tucker, R.D., O'Brien, P.J., Krogh, T.E., 2003. Coesite inclusions and the U–Pb age of zircons from the Hareidland Eclogite in the Western Gneiss Region of Norway. Lithos 67, 181–190. http://dx.doi.org/10.1016/S0024-4937(03)00014-8.
Cuthbert, S.J., Carswell, D.A., Krogh-Ravna, E.J., Wain, A., 2000. Eclogites and eclogites in the Western Gneiss Region, Norwegian Caledonides. Lithos 52, 165–195. http://dx.doi.org/10.1016/S0024-4937(99)00090-0.
Dallmeyer, R.D., Johansson, L., Möller, C., 1992. Chronology of Caledonian high-pressure granulite-facies metamorphism, uplift, and deformation within northern parts of the Western Gneiss Region, Norway. Geological Society of America Bulletin 104, 444–455.
DesOrmeau, J.W., Gordon, S.M., Kylander-Clark, A.R.C., Hacker, B.R., Bowring, S.A., Schoene, B., Samperton, K.M., 2015. Insights into (U)HP metamorphism of the Western Gneiss Region, Norway: a high-spatial resolution and high-precision zircon study. Chemical Geology 414, 138–155.
Dewey, J.F., Strachan, R.A., 2003. Changing Silurian–Devonian relative plate motion in the Caledonides: sinistral transpression to sinistral transtension. Journal of the Geological Society 160, 219–229.
Dobrzhinetskaya, L.F., Eide, E.A., Larsen, R.B., Sturt, B.A., Trønnes, R.G., Smith, D.C., Taylor, W.R., Posukhova, T.V., 1995. Microdiamond in high-grade metamorphic rocks of the Western Gneiss region, Norway. Geology 23, 597–600. http://dx.doi.org/10.1130/0091-7613(1995)023<0597:MIHGMR>2.3.CO;2.
Essex, R.M., Gromet, L.P., Andréasson, P.-G., Albrecht, L.G., 1997. Early Ordovician U–Pb metamorphic ages of the eclogite-bearing Seve Nappes, northern Scandinavian Caledonides. Journal of Metamorphic Geology 15, 665–676.
Fossen, H., 2000. Extensional tectonics in the Caledonides: synorogenic or postorogenic? Tectonics 19, 213–224.
Fossen, H., 2010. Extensional tectonics in the North Atlantic Caledonides: a regional view. In: Law, R.D., Butler, R.W.H., Holdsworth, R.E., Krabbendam, M., Strachan, R.A. (Eds.), Continental Tectonics and Mountain Building: The Legacy of Peach and Horne. Geological Society, London, Special Publications 335, pp. 767–793.
Fossen, H., Dunlap, W.J., 1998. Timing and kinematics of Caledonian thrusting and extensional collapse, southern Norway: evidence from 40Ar/39Ar thermochronology. Journal of Structural Geology 20, 765–781.
Fossen, H., Teyssier, C., Whitney, D.L., 2013. Transtensional folding. Journal of Structural Geology 56, 89–102.
Ganzhorn, A.C., Labrousse, L., Prouteau, G., Leroy, C., Vrijmoed, J.C., Andersen, T.B., Arbaret, L., 2014. Structural, petrological and chemical analysis of syn-kinematic migmatites: insights from the Western Gneiss Region, Norway. Journal of Metamorphic Geology 32, 647–673.
Gee, D.G., 1975. A tectonic model for the central part of the Scandinavian Caledonides. American Journal of Science 275A, 468–515.
Gee, D.G., 1980. Basement-cover relationships in the central Scandinavian Caledonides. Geologiska Föreningens i Stockholm Förhandlingar 102, 455–474.
Gee, D.G., Janák, M., Majka, J., Robinson, P., van Roermund, H., 2013. Subduction along and within the Baltoscandian margin during closing of the Iapetus Ocean and Baltica–Laurentia collision. Lithosphere 5, 169–178.
Gilotti, J.A., Hull, J.M., 1993. Kinematic stratification in the hinterland of the central Scandinavian Caledonides. Journal of Structural Geology 15, 629–646.
Glodny, J., Kühn, A., Austrheim, H., 2008. Diffusion versus recrystallization processes in Rb–Sr geochronology: isotopic relicts in eclogite facies rocks, Western Gneiss Region, Norway. Geochimica et Cosmochimica Acta 72, 506–525. http://dx.doi.org/10.1016/j.gca.2007.10.021.
Gordon, S.M., Whitney, D.L., Teyssier, C., Fossen, H., 2013. U–Pb dates and trace-element geochemistry of zircon from migmatite, Western Gneiss Region, Norway: significance for history of partial melting in continental subduction. Lithos 170–171, 35–53. http://dx.doi.org/10.1016/j.lithos.2013.02.003.
Griffin, W.L., Brueckner, H.K., 1980. Caledonian Sm–Nd ages and a crustal origin for Norwegian eclogites. Nature 285, 319–321. http://dx.doi.org/10.1038/285319a0.
Griffin, W.L., Brueckner, H.K., 1985. REE, Rb–Sr and Sm–Nd studies of Norwegian eclogites. Chemical Geology 52, 249–271. http://dx.doi.org/10.1016/0168-9622(85)90021-1.
Hacker, B.R., 2006. Pressures and temperatures of ultrahigh-pressure metamorphism: implications for UHP tectonics and H_2O in subducting slabs. International Geology Review 48, 1053–1066.
Hacker, B.R., 2007. Ascent of the ultrahigh-pressure Western Gneiss Region, Norway. Geological Society of America Special Paper 419, 171–184.
Hacker, B.R., Gans, P.B., 2005. Continental collisions and the creation of ultrahigh-pressure terranes: petrology and thermochronology of nappes in the central Scandinavian Caledonides. Geological Society of America Bulletin 117, 117–134. http://dx.doi.org/10.1130/B25549.1.
Hacker, B.R., Andersen, T.B., Johnston, S., Kylander-Clark, A.R.C., Peterman, E.M., Walsh, E.O., Young, D., 2010. High-temperature deformation during continental-margin subduction and exhumation: the ultrahigh-pressure Western Gneiss Region of Norway. Tectonophysics 480 (1–4), 149–171. http://dx.doi.org/10.1016/j.tecto.2009.08.012.
Hacker, B.R., Kylander-Clark, A.R.C., Holder, R., Andersen, T.B., Peterman, E.M., Walsh, E.O., Munnikhuis, J.K., 2015. Monazite response to ultrahigh-pressure subduction from U–Pb dating of laser ablation split stream. Chemical Geology 409, 28–41.
Harley, S.L., Kinny, P., Snape, I., Black, L.P., 2001. Zircon chemistry and the definition of events in Archean granulite terrains. In: Fourth International Archean Symposium, Extended Abstract Volume. AGSO Geoscience Australia Record 2001 (37), 511–513.
Hokada, T., Harley, S.L., 2004. Zircon growth in UHT leucosome: constraints from zircon–garnet rare earth elements (REE) relations in Napier Complex, East Antarctica. Journal of Mineralogical and Petrological Sciences 99, 180–190. http://dx.doi.org/10.2465/jmps.99.180.
Holder, R.M., Hacker, B.R., Kylander-Clark, A.R.C., Cottle, J.M., 2015. Monazite trace-element and isotopic signatures of (ultra)high-pressure metamorphism: examples from the Western Gneiss Region, Norway. Chemical Geology 409, 99–111.
Hollocher, K., Robinson, P., Terry, M.P., Walsh, E., 2007. Application of major- and trace-element geochemistry to refine U–Pb zircon, and Sm/Nd or Lu/Hf sampling targets for geochronology of HP and UHP eclogites, Western Gneiss Region, Norway. American Mineralogist 92, 1919–1924. http://dx.doi.org/10.2138/am.2007.2405.
Janák, M., Ravna, E.J.K., Kullerud, K., Yoshida, K., Milovsky, R., Hirajima, T., 2013. Discovery of diamond in the Tromsø Nappe, Scandinavian Caledonides (N. Norway). Journal of Metamorphic Geology 31, 691–703. http://dx.doi.org/10.1111/jmg.12040.
Johansson, L., Möller, C., 1986. Formation of sapphirine during retrogression of a basic high-pressure granulite, Roan, Western Gneiss Region, Norway. Contributions to Mineralogy and Petrology 94, 29–41.
Johnston, S.M., Hacker, B.R., Andersen, T.B., 2007. Exhuming Norwegian ultrahigh-pressure rocks: overprinting extensional structures and the role of the Nordfjord–Sogn detachment zone. Tectonics 26. http://dx.doi.org/10.1029/2005TC001933.
Kelly, N.M., Harley, S.L., 2005. An integrated microtextural and chemical approach to zircon geochronology: refining the Archaean history of the Napier Complex, east Antarctica. Contributions to Mineralogy and Petrology 149, 57–84. http://dx.doi.org/10.1007/s00410-004-0635-6.
Kjerulf, T., 1871. Om Trondheims stifts geologi. Nyt. Mag. For Naturv. Christiania 18, 1–79.
Krabbendam, M., Dewey, J.F., 1998. Exhumation of UHP rocks by transtension in the Western Gneiss Region, Scandinavian Caledonides. In: Holdsworth, R.E., et al. (Eds.) Continental transpressional and transtensional tectonics. Geological Society of London, Special Publication 135, 159–181.
Krill, A.G., 1980. Tectonics of the Oppdal area, central Norway. Geologiska Föreningens i Stockholm Förhandlingar 102, 523–530.
Krogh, E.J., 1977. Evidence for Precambrian continent–continent collision in western Norway. Nature 267, 17–19. http://dx.doi.org/10.1038/267017a0.
Krogh, T.E., Kamo, S.L., Robinson, P., Terry, M.P., Kwok, K., 2011. U–Pb zircon geochronology of eclogites from the Scandian Orogen, northern Western Gneiss Region, Norway: 14–20 million years between eclogite crystallization and return to amphibolite-facies conditions. Canadian Journal of Earth Sciences 48 (2), 441–472. http://dx.doi.org/10.1139/E10-076.
Kylander-Clark, A.R.C., Hacker, B.R., 2014. Age and significance of felsic dikes from the UHP Western Gneiss Region. Tectonics 33. http://dx.doi.org/10.1002/2014TC003582.
Kylander-Clark, A.R.C., Hacker, B.R., Johnson, C.M., Beard, B.L., Mahlen, N.J., Lapen, T.J., 2007. Coupled Lu–Hf and Sm–Nd geochronology constrains prograde and exhumation histories of high- and ultrahigh-pressure eclogites from western Norway. Chemical Geology 242, 137–154.
Kylander-Clark, A.R.C., Hacker, B.R., Mattinson, J.M., 2008. Slow exhumation of UHP terranes: titanite and rutile ages of the Western Gneiss Region, Norway. Earth and Planetary Science Letters 272 (3–4), 531–540. http://dx.doi.org/10.1016/j.epsl.2008.05.019.
Kylander-Clark, A.R.C., Hacker, B.R., Johnson, C.M., Beard, B.L., Mahlen, N.J., 2009. Slow subduction of a thick ultrahigh-pressure terrane. Tectonics 28. http://dx.doi.org/10.1029/2007TC002251.
Kylander-Clark, A.R.C., Hacker, B.R., Cottle, J.M., 2013. Laser-ablation split-stream ICP petrochronology. Chemical Geology 345, 99–112. http://dx.doi.org/10.1016/j.chemgeo.-2013.02.019.
Labrousse, L., Jolivet, L., Agard, P., Hébert, R., Andersen, T.B., 2002. Crustal-scale boudinage and migmatization of gneiss during their exhumation in the UHP province of Western Norway. Terra Nova 14, 263–270.
Labrousse, L., Prouteau, G., Ganzhorn, A.C., 2011. Continental exhumation triggered by partial melting at ultrahigh pressure. Geology 39, 1171–1174. http://dx.doi.org/10.1130/-G32316.1.
Ladenberger, A., Be'eri-Shlevin, Y., Claesson, S., Gee, D.G., Majka, J., Romanova, I.V., 2014. Tectonometamorphic evolution of the Åreskutan Nappe-Caledonian history revealed by SIMS U–Pb zircon geochronology. In: Corfu, F., Gasser, D., Chew, D.M. (Eds.), New perspectives on the Caledonides of Scandinavia and Related Areas. Geological Society, London, Special Publications 390.
Majka, J., Be'eri-Shlevin, Y., Gee, D.G., Ladenberger, A., Claesson, S., Konecny, P., Klonowksa, I., 2012. Multiple monazite growth in the Åreskutan migmatite: evidence for a polymetamorphic Late Ordovician to Late Silurian evolution in the Seve Nappe Complex of west-central Jämtland, Sweden. Journal of Geosciences 57, 3–23.
Majka, J., Rosén, Å., Janák, M., Froitzheim, N., Klonowska, I., Manecki, M., Sasinková, V., Yoshida, K., 2014. Microdiamond discovered in the Seve Nappe (Scandinavian Caledonides) and its exhumation by the "vacuum-cleaner" mechanism. Geology 42, 1107–1110.

McLean, N.M., Bowring, J.F., Bowring, S.A., 2011. An algorithm for U–Pb isotope dilution data reduction and uncertainty propagation. Geochemistry, Geophysics, Geosystems 12, Q0AA18. http://dx.doi.org/10.1029/2010GC003478.
Möller, C., 1988. Geology and metamorphic evolution of the Roan area, Vestranden, Western Gneiss Region, Central Norwegian Caledonides. NGU Bulletin 413, 1–31.
Monteleone, B.D., Baldwin, S.L., Webb, L.E., Fitzgerald, P.G., Grove, M., Schmitt, A.K., 2007. Late Miocene–Pliocene eclogite facies metamorphism, D'Entrecasteaux Islands, SE Papua New Guinea. Journal of Metamorphic Geology 25, 245–265. http://dx.doi.org/10.1111/j.1525-1314.2006.00685.x.
Mørk, M.B.E., Kullerud, K.V., Stabel, A., 1988. Sm–Nd dating of Seve eclogites, Norrbotten, Sweden: evidence for early Caledonian (505 Ma) subduction. Contributions to Mineralogy and Petrology 99, 344–351. http://dx.doi.org/10.1007/BF00375366.
Norton, M.G., 1986. Late Caledonian extension in western Norway: a response to extreme crustal thickening. Tectonics 5, 195–204.
Norton, M.G., 1987. The Nordfjord–Sogn detachment, W. Norway. Norsk Geologisk Tidsskrift 67, 93–106.
Osmundsen, P.T., Andersen, T.B., Markussen, S., Svendby, A.K., 1998. Tectonics and sedimentation in the hanging wall of a major extensional detachment: The Devonian Kvamshesten basin, western Norway. Basin Research 10, 213–234.
Osmundsen, P.T., Eide, E.A., Haabesland, N.E., Roberts, D., Andersen, T.B., Kendrick, M., Bingen, B., Braathen, A., Redfield, T.F., 2006. Kinematics of the Høybakken detachment zone and the Møre–Trøndelag Fault Complex, central Norway. Journal of the Geological Society, London 163, 303–318.
Ramberg, H., 1943. En undersøkelse av Vestrandens regionalmetamorfe bergarter. Norsk Geologisk Tidsskrift 23, 1–174.
Ramberg, H., 1966. The Scandinavian Caledonides as studied by centrifuged dynamic models. Bulletin of the Geological Institutions of Uppsala 43, 1–72.
Ravna, E.J.K., Terry, M.P., 2004. Geothermobarometry of UHP and HP eclogites and schists—an evaluation of equilibria among garnet–clinopyroxene–kyanite–phengite–coesite/quartz. Journal of Metamorphic Geology 22, 579–592. http://dx.doi.org/10.1111/j.1525-1314.2004.00534.x.
Renedo, R.N., Nachlas, W.O., Whitney, D.L., Teyssier, C., Piazolo, S., Gordon, S.M., Fossen, H., 2015. Fabric development during exhumation from ultrahigh-pressure in an eclogite-bearing shear zone, Western Gneiss Region, Norway. Journal of Structural Geology http://dx.doi.org/10.1016/j.jsg.2014.09.012.
Roberts, D., 1983. Devonian tectonic deformation in the Norwegian Caledonides and its regional perspectives. Norges Geologiske Undersøkelse 380, 85–96.
Roberts, D., 2003. The Scandinavian Caledonides: Event chronology, palaeogeographic settings and likely modern analogues. Tectonophysics 365, 283–299. http://dx.doi.org/10.1016/-S0040-1951(03)00026-X.
Roberts, D., Gee, D.G., 1985. An introduction to the structure of the Scandinavian Caledonides. In: Gee, D.G., Sturt, B.A. (Eds.), The Caledonide Orogen—Scandinavia and related areas. Wiley, Chichester, UK, pp. 55–68.
Robinson, P., 1995. Extension of Trollheimen tectonostratigraphic sequence in deep synclines near Molde and Brattvåg, Western Gneiss Region, southern Norway. Norsk Geologisk Tidsskrift 75, 181–197.
Robinson, P., Hollocher, K., 2008. Geology of Trollheimen. In: Robinson, P., Roberts, D., Gee, D.G. (Eds.), Guidebook: a tectonostratigraphic transect across the central Scandinavian CaledonidesNGU report 2008.064, pt. II. Geological Survey of Norway, Trondheim, pp. 6-1–6-7.
Root, D., Corfu, F., 2012. U–Pb geochronology of two discrete Ordovician high-pressure metamorphic events in the Seve Nappe Complex, Scandinavian Caledonides. Contributions to Mineralogy and Petrology 163, 769–788.
Root, D.B., Hacker, B.R., Mattinson, J.M., Wooden, J.L., 2004. Zircon geochronology and ca. 400 Ma exhumation of Norwegian ultrahigh-pressure rocks: an ion microprobe and chemical abrasion study. Earth and Planetary Science Letters 228, 325–341. http://dx.doi.org/10.1016/-j.epsl.2004.10.019.
Root, D.B., Hacker, B.R., Gans, P.B., Ducea, M.N., Eide, E.A., Mosenfelder, J.L., 2005. Discrete ultrahigh-pressure domains in the Western Gneiss Region, Norway: implications for formation and exhumation. Journal of Metamorphic Geology 23, 45–61. http://dx.doi.org/10.1111/-j.1525-1314.2005.00561.x.
Rosenberg, C.L., Handy, M.R., 2005. Experimental deformation of partially melted granite revisited: implications for the continental crust. Journal of Metamorphic Geology 23, 19–28.
Rubatto, D., 2002. Zircon trace element geochemistry: distribution coefficients and the link between U–Pb ages and metamorphism. Chemical Geology 184, 123–138. http://dx.doi.org/10.1016/S0009-2541(01)00355-2.
Rubatto, D., Hermann, J., 2003. Zircon formation during fluid circulation in eclogites (Monviso, Western Alps): implications for Zr and Hf budget in subduction zones. Geochimica et Cosmochimica Acta 67, 2173–2187. http://dx.doi.org/10.1016/S0016-7037(02)01321-2.
Rubatto, D., Hermann, J., 2007. Experimental zircon/melt and zircon/garnet trace element partitioning and implications for the geochronology of crustal rocks. Chemical Geology 241, 38–61. http://dx.doi.org/10.1016/j.chemgeo.2007.01.027.
Rutter, E., Neumann, D., 1995. Experimental deformation of partially molten Westerly granite under fluid-absent conditions, with implications for the extraction of granitic magmas. Journal of Geophysical Research 100, 15697–15715.
Scambelluri, M., Pettke, T., van Roermund, H.L.M., 2008. Majoritic garnets monitor deep subduction fluid flow and mantle dynamics. Geology 36, 59–62.
Schärer, U., Labrousse, L., 2003. Dating the exhumation of UHP rocks and associated crustal melting in the Norwegian Caledonides. Contributions to Mineralogy and Petrology 144, 758–770. http://dx.doi.org/10.1007/s00410-002-0428-8.
Schouenborg, B.E., 1988. U/Pb-zircon datings of Caledonian cover rocks and cover-basement contacts, northern Vestranden, central Norway. Norsk Geologisk Tidsskrift 68, 75–87.
Schouenborg, B., Borås, Johansson, Gorbatschiev, L., Lund, R., 1991. U/Pb zircon ages of basement gneisses and discordant felsic dykes from Vestranden, westernmost Baltic Shield and central Norwegian Caledonides. Geologische Rundschau 80 (1), 121–134.
Séranne, M., 1992. Late Palaeozoic kinematics of the Møre–Trøndelag Fault Zone and adjacent areas, Central Norway. Norsk Geologisk Tidsskrift 72, 141–158.
Séranne, M., Seguret, M., 1987. The Devonian basins of western Norway: tectonics and kinematics of an extending crust. Geological Society, London, Special Publications 28, 537–548.
Spencer, K.J., Hacker, B.R., Kylander-Clark, A.R.C., Andersen, T.B., Cottle, J.M., Stearns, M.A., Poletti, J.E., Seward, G.G.E., 2013. Campaign style titanite U–Pb dating by laser-ablation ICP: implications for crustal flow, phase transformations and titanite closure. Chemical Geology 341, 84–101. http://dx.doi.org/10.1016/j.chemgeo.2012.11.012.
Stephens, M.B., van Roermund, H.L.M., 1984. Occurrence of glaucophane and crossite in eclogites of the Seve Nappes, southern Norrbotten Caledonides, Sweden. Norsk Geologisk Tidsskrift 69, 155–163.
Straume, A.K., Austrheim, H., 1999. Importance of fracturing during retro-metamorphism of eclogites. Journal of Metamorphic Geology 17, 637–652.
Sun, S.S., McDonough, W.F., 1989. Chemical and isotopic systematics of oceanic basalts: implications for mantle composition and processes. Geological Society of London, Special Publication 42, 313–345. http://dx.doi.org/10.1144/GSL.SP.1989.042.01.19.
Taylor, R.J.M., Harley, S.L., Hinton, R.W., Elphick, S., Clark, C., Kelly, N.M., 2014. Experimental determination of REE partition coefficients between zircon, garnet, and melt: a key to understanding high-temperature crustal processes. Journal of Metamorphic Geology http://dx.doi.org/10.1111/jmg.12118.
Terry, M.P., Robinson, P., Ravna, E.J.K., 2000a. Kyanite eclogite thermobarometry and evidence for thrusting of UHP over HP metamorphic rocks, Nordøyane, Western Gneiss Region, Norway. American Mineralogist 85, 1637–1650.
Terry, M.P., Robinson, P., Hamilton, M.A., Jercinovic, M.J., 2000b. Monazite geochronology of UHP and HP metamorphism, deformation, and exhumation, Nordøyane, Western Gneiss Region, Norway. American Mineralogist 85, 1651–1664.
Torsvik, T.H., Smethurst, M.A., Meert, J.G., Vandervoo, R., McKerrow, W.S., Brasier, M.D., Sturt, B.A., Walderhaug, H.J., 1996. Continental break-up and collision in the Neoproterozoic and Palaeozoic — A tale of Baltica and Laurentia. Earth-Science Reviews 40, 229–258.
Tucker, R.D., 1986. Geology of the Hemnefjord–Orkanger area, south central Norway. Norges Geologiske Undersøkelse 404, 1–20.
Tucker, R.D., Boyd, R., Barnes, S.-J., 1990. A U–Pb zircon age for the Råna intrusion, N. Norway: New evidence of basic magmatism in the Scandinavian Caledonides in Early Silurian time. Norsk Geologisk Tidsskrift 70, 229–239.
Tucker, R.D., Robinson, P., Solli, A., Gee, D.G., Thorsnes, T., Krogh, T.E., Nordgulen, Ø., Bickford, M.E., 2004. Thrusting and extension in the Scandian hinterland, Norway: New U–Pb ages and tectonostratigraphic evidence. American Journal of Science 304 (6), 477–532. http://dx.doi.org/10.2475/ajs.304.6.477.
van Roermund, H.L.M., 1985. Eclogites of the Seve Nappe, central Scandinavian Caledonides. In: Gee, D.G., Sturt, B.A. (Eds.), The Caledonide orogen–Scandinavia and related areas. John Wiley & Sons, Chichester, UK, pp. 873–886.
van Roermund, H.L.M., 2009. Recent progress in Scandian ultrahigh-pressure metamorphism in the northernmost domain of the Western Gneiss Complex, SW Norway: continental subduction down to 180–200 km depth. Journal of the Geological Society 166, 739–751.
van Roermund, H.L.M., Bakker, E., 1984. Structure and metamorphism of the Tangen-Inviken area, Seve Nappes, central Scandinavian Caledonides. Geologiska Föreningens i Stockholm Förhandlingar 105, 301–319.
van Roermund, H.L.M., Drury, M.R., 1998. Ultra-high pressure (P > 6 GPa) garnet peridotites in western Norway: exhumation of mantle rocks from >185 km depth. Terra Nova 10, 295–301.
Vrijmoed, J.C., Van Roermund, H.L.M., Davis, G.R., 2006. Evidence for diamond-grade ultrahigh-pressure metamorphism and fluid interaction in the Svartberget Fe–Ti garnet peridotite-websterite body, Western Gneiss Region, Norway. Mineralogy and Petrology 88, 381–405. http://dx.doi.org/10.1007/s00710-006-0160-6.
Wain, A., 1997. New evidence for coesite in eclogite and gneisses: Defining an ultrahigh-pressure province in the Western Gneiss region of Norway. Geology 25, 927–930 (http-://dx.doi.org/0.1130/0091-7613(1997) 025 < 0927:NEFCIE > 2.3.CO;2).
Walsh, E.O., Hacker, B.R., Gans, P.B., Grove, M., Gehrels, G., 2007. Protolith ages and exhumation histories of (ultra)high-pressure rocks across the Western Gneiss Region, Norway. Journal of Metamorphic Geology 119, 289–301.
Walsh, E.O., Hacker, B.R., Gans, P.B., Wong, M.S., Andersen, T.B., 2013. Crustal exhumation of the Western Gneiss Region UHP terrane, Norway: $^{40}Ar/^{39}Ar$ thermochronology and fault-slip analysis. Tectonophysics 608, 1159–1179.
Whitehouse, M.J., Platt, J.P., 2003. Dating high-grade metamorphism—constraints from rare-earth elements in zircon and garnet. Contributions to Mineralogy and Petrology 145, 61–74. http://dx.doi.org/10.1007/s00410-002-0432-z.
Wolff, F.C., 1976. Geologisk kart over Norge, berggrunnskart Trondheim 1:250 000. Norges Geologiske Undersøkelse.
Young, D.J., Hacker, B.R., Andersen, T.B., Corfu, F., 2007. Prograde amphibolite facies to ultrahigh-pressure transition along Nordfjord, western Norway: implications for exhumation tectonics. Tectonics 26, TC1007. http://dx.doi.org/10.1029/2004TC001781.